

University of Southern Queensland
Faculty of Health, Engineering & Sciences

**Investigation of Millimetre FMCW Radar for Improved
Situational Awareness for Fire Fighting Vehicles**

A dissertation submitted by

Matthew Barrett

in fulfilment of the requirements of

ENG4112 Research Project

towards the degree of

Bachelor of Engineering (Honours) Mechatronics

Submitted: October, 2020

Abstract

The importance of situational awareness during a bush fire has long been a concern and emphasis among the firefighting community. Until recently, mitigation against low situation awareness has been addressed by experience, in-depth training, and mentoring. Emerging technologies and sensing systems have a role to play in addressing the issue. However, without in-depth empirical evidence demonstrating the effectiveness of such a system in a bush fire, they will not be trusted by the firefighting community.

Millimetre frequency modulated continuous wave (FMCW) radar is one possible option for improving fire crews' situational awareness during a bush fire. With recent developments in automotive radar technology, sensors capable of detecting objects with high accuracy are now readily available and affordable. Measurement capabilities include accurate range, bearing, elevation, velocity and return intensity (radar cross section) at a distance greater than 50 meters. The technology is insensitive to environmental influences such as smoke, fog, rain, poor lighting, or extreme temperatures. Alone, or combined with other sensor technology such as infrared imaging, will allow object identification in high temperature, dense smoke environments, therefore improving risk awareness.

A Texas Instruments (TI) IWR1443 mm-wave development board along with ROS (Robot Operating System) was used to evaluate the viability of mm-wave radar for fire fighting situational awareness. Experiments were performed to evaluate (1) the maximum detectable range of typical objects / obstacles encountered in these situations, (2) the horizontal antenna pattern of the IWR1443 sensor, and (3) radar cross-section measurements of a standing and fallen gum tree (the most common cause of the collision in firefighting vehicles), along with the maximum detectable range of a standing tree. Results are validated against published TI results, and where possible, simulated against standard theoretical tools used for radar system design.

Results show the IWR1443 can detect objects with millimetre accuracy at a range greater than fifty meters, with a -3dB beamwidth of approximately ± 30 degrees. Range results were evaluated against the commonly used radar range equation to determine the range predictability of a known RCS. Results are not comparable to the simulated results of the radar range equation. However, utilising the range calibration and antenna pattern data from this study, it is possible to evaluate the expected return intensity of a known RCS at a specified angle. Finally, radar cross-section experiments of both a standing and fallen tree, show an RCS of approximately 60 m^2 with a maximum detectable range of 45m.

Informing future sensor system design, it was concluded that mm-wave radar sensing can accurately detect and differentiate multiple objects at a long-range with a wide field of view. Further, using RCS measurements taken of a standing and fallen gum tree, it can be shown that radar sensing data alone cannot determine the orientation of a tree, and therefore the risk it presents to fire fighting vehicles. Finally, it was demonstrated that radar system design tools such as the radar range equation cannot be used with certainty, meaning an empirical approach is required when designing for any non-standard application.

University of Southern Queensland
Faculty of Health, Engineering & Sciences

ENG4111/2 *Research Project*

Limitations of Use

The Council of the University of Southern Queensland, its Faculty of Health, Engineering & Sciences, and the staff of the University of Southern Queensland, do not accept any responsibility for the truth, accuracy or completeness of material contained within or associated with this dissertation.

Persons using all or any part of this material do so at their own risk, and not at the risk of the Council of the University of Southern Queensland, its Faculty of Health, Engineering & Sciences or the staff of the University of Southern Queensland.

This dissertation reports an educational exercise and has no purpose or validity beyond this exercise. The sole purpose of the course pair entitled “Research Project” is to contribute to the overall education within the student’s chosen degree program. This document, the associated hardware, software, drawings, and other material set out in the associated appendices should not be used for any other purpose: if they are so used, it is entirely at the risk of the user.

Dean

Faculty of Health, Engineering & Sciences

Certification of Dissertation

I certify that the ideas, designs and experimental work, results, analyses and conclusions set out in this dissertation are entirely my own effort, except where otherwise indicated and acknowledged.

I further certify that the work is original and has not been previously submitted for assessment in any other course or institution, except where specifically stated.

MATTHEW BARRETT



Acknowledgments

I would like to thank my supervisor, Craig Lobsey for helping me over a few hurdles I faced along the way and just generally being a great mentor. Thank you to my colleague Liam McQuellin, for helping me overcome a few programming issues. Finally, I would like to thank my wife, Alisha. You believed in me from the day I started my engineering degree. Even with all the time I had to spend away from you and our 2 girls, you always supported me to keep going. I would not have made it without you. Thank you.

MATTHEW BARRETT

Contents

Abstract	i
Acknowledgments	v
List of Figures	xi
List of Tables	1
Chapter 1 Introduction	1
1.1 Outline of the Study	1
1.2 Background	2
1.3 The Problem	4
1.4 Research Aims & Objectives	4
Chapter 2 Literature Review	6
2.1 Chapter Overview	6
2.2 Fundamentals of Situational Awareness in a Fire Environment	6
2.3 Basic Examination of Sensor Technologies to Improve Situational Awareness in a Fire Environment	7

2.4	Sensor Fusion for Increased Situational Awareness	11
2.4.1	Fusion of mm-Wave Radar with Machine Vision	11
2.5	Fundamentals of Millimetre FMCW Sensing	12
2.6	FMCW Radar Range & Angle Measurements	15
2.6.1	Radar Range Measurement	15
2.6.2	Radar Angle Detection	18
2.6.3	Maximum Angular Field of View	19
2.7	Radar Cross Section Measurements	19
2.8	Conclusions	21
Chapter 3 Methodology		23
3.1	Radar Sensor Selection	23
3.2	Chirp Parameters	24
3.2.1	Data Collection using ROS (Robot Operating System)	27
3.3	Triangular RCS Target	28
3.4	Maximum Detectable Range	30
3.5	Peripheral Sensing Capabilities	31
3.6	Radar Cross Section Measurements	32
3.7	Data Processing	33
Chapter 4 Results & Discussion		34
4.1	Initial Testing	34

4.2	Range Capabilities	36
4.2.1	Return Intensity	36
4.2.2	Range Accuracy and Resolution	39
4.3	Peripheral Capabilities	40
4.4	Radar Cross Section Measurements	42
4.5	Object Identification & Range Prediction	46
4.5.1	Detecting Range of Standing Tree	46
4.5.2	Object Identification	48
4.5.3	Range Prediction using RRE	48
4.6	Discrete Discussion	51
Chapter 5 Conclusions & Future Work		52
5.1	Introduction	52
5.2	Maximum Detectable Range and Peripheral Capabilities	52
5.3	Radar Cross Section Measurements	53
5.4	Future Work	54
References		55
Chapter 6 Project Specification		59
Chapter 7 Radiation Safety Assessment		62
7.1	Risk Management Calculations	63

Chapter 8 Results utilising Mid-Range Chirp Parameters	65
8.1 Introduction	66
8.2 Mid-Range Chirp Parameters	66
8.3 Results	67
8.4 Results - Small Corner Reflectors	70
Chapter 9 Post Processing Example Code	72
Chapter 10 Project Timeline	74
Chapter 11 Risk Management Form	76

List of Figures

1.1	Data produced by the Bureau of Meteorology shows a warming of 1.5 degrees since 1950 (of Meteorology n.d.).	2
2.1	With a target object at 1.8m, data points display the attenuation due to smoke of the 4 selected sensors (Starr & Lattimer 2014).	10
2.2	To identify objects the radar profile takes into account signal intensity. The signal intensity is dependant on the shape size and material properties of the reflected object (Omine, Sakai, Aoki & Takagi 2004)	10
2.3	Transmit and receive wave forms for a FMCW radar with a stationary target using a saw-tooth wave.	12
2.4	The relationship between frames, loops and chirps Constapel, Cimdins, Hellbrück & Lübeck (2019)	14
2.5	Chirp signal, with frequency as a function of time (Falconbridge 2002)	15
2.6	FMCW Range Ambiguity. Reproduced from (Falconbridge 2002)	17
2.7	Estimating AoA with two antennas. Reproduced from (Rao, S 2017)	18
2.8	Radar return intensity of a typical car. (Buddendick & Eibert 2010)	20
3.1	Texas Instruments IWR1443 Boost mm-wave FMCW Radar Sensor (<i>IWR1443BOOST Evaluation Module mm-Wave Sensing Solution</i> 2018)	24

3.2	Chirp parameter configuration for TI mm-wave devices (Texas Instruments 2018)	26
3.3	Basic Architecture of the ROS Environment	27
3.4	Triangular corner reflector. Reproduced from (Tutorial 2020)	28
3.5	The fabrication of triangular corner reflectors was completed on a precision welding table using the GTAW method.	29
3.6	Site selection for maximum detectable range and angular resolution experiments	30
3.7	Experimental schematic for determining maximum detectable range	31
3.8	Beam width calibration	32
3.9	Radar cross section of various trees	33
4.1	Radar data visualised	35
4.2	Triangular corner reflector	36
4.3	Maximum detectable range of fabricated corner reflectors	37
4.4	The signal loss due to angular misalignment increase with distance according to expression 4.1	38
4.5	Range accuracy and resolution when measuring largest corner reflector, T1. Data includes uncertainty and the range error recorded by the radar at each location.	39
4.6	Experimentally measured and fitted horizontal antenna pattern against the same results published by Texas Instruments after digitising	41
4.7	Standing tree selected for RCS and range measurements. The orientation of the tree relative to the result is also shown.	43
4.8	Radar Cross Section measurement of standing tree in dBsm	43

4.9	Fallen tree selected for RCS measurements. The orientation of the tree relative to the result is also shown.	44
4.10	Radar cross section measurement of fallen tree in dBsm	44
4.11	Range measurement best fit of known RCS's	46
4.12	Radar data visualised	47
4.13	Theoretical and experimental range comparison using the Radar Range Equation. In this instance, a 4th order fit was used to demonstrate the linearisation after 25 meters.	50
8.1	Maximum detectable range of the corner reflectors using mid range chirp parameters	67
8.2	Experimental result of maximum detectable range of a utility vehicle using mid-range chirp parameters	68
8.3	Experiment evaluating the maximum detectable range of a utility using mid-range chirp parameters.	68
8.4	Range accuracy using mid-midrange chirp parameters.	69
8.5	evaluation of maximum detectable range and the uncertainty using mid-range chirp parameters and small RCS corner reflectors	70
8.6	Calibration of maximum detectable range using mid-range chirp parameters and small RCS corner reflectors	71

List of Tables

2.1	Summary of sensor performance to see through two extremes of smoke. (Starr & Lattimer 2014)	9
3.1	Summary of chirp parameters, and resulting radar accuracy and resolution. Parameters were specified using TI's Demo Visualiser software.	26
3.2	Tabulated triangular corner reflector calculations based on equation 3.1	29
4.1	Summary of corner reflector manufacturing error	36
4.2	Tree type and physical size of standing and fallen tree	42
4.3	Radar parameters for experimental validation.	49
7.1	Basic restrictions for time averaged and instantaneous incident power flux density (<i>Radiation Protection Standard</i> 2002)	64
8.1	Summary of chirp parameters, and resulting radar accuracy and resolution	66
8.2	Tabulated triangular corner reflector calculations based on equation 3.1. The listed RCS are smaller than those used in chapter 4.	70

Chapter 1

Introduction

'Australia is a fire prone country. Bush fires have been a feature of the Australian environment for at least 65 million years and will continue to feature in the future'(Bradstock n.d.)

1.1 Outline of the Study

The recent 2020 Australian bush fire season adds new perspective to the above statement. Not only can the Australian people and firefighting communities expect to encounter large scale bush fires, but they can also expect them to increase in severity. The 2020 bush fire season was the most severe on record, amplified by a significant drought and globally increasing temperatures. To manage these fires required thousands of volunteer and professional firefighters to risk their lives to save property and life from unprecedented destruction. This research was motivated by the stories of lives lost in Australian bush fires with the aim of minimising similar incidents occurring in the future. The purpose and scope of this study outlining how this will be achieved is discussed in section 1.4 Research Aims & Objectives.

1.2 Background

The Australian continent has a hot and dry climate and wildfires are a natural part of the ecosystem. The New South Wales (NSW) statutory bush fire danger period runs from the 1st of October until the 31st of March the following year. However, this can vary depending on local conditions and climate forecasts (*Bush Fire Danger Period and Fire Permits* n.d.). In recent years bush fires have steadily become more severe, impacting a larger population and requiring a more extensive response. Modelling performed by the Bureau of Meteorology (BoM) found that 2019 was the hottest year on record and temperatures have steadily been increasing above the mean since the late 1950s. This is shown in figure 1.1 produced by the BoM. With this in mind, it is no surprise the Australian 2019-2020 bush fire season ran for a much longer period, with bush fires reported as early as June and the season finally ending in late February.

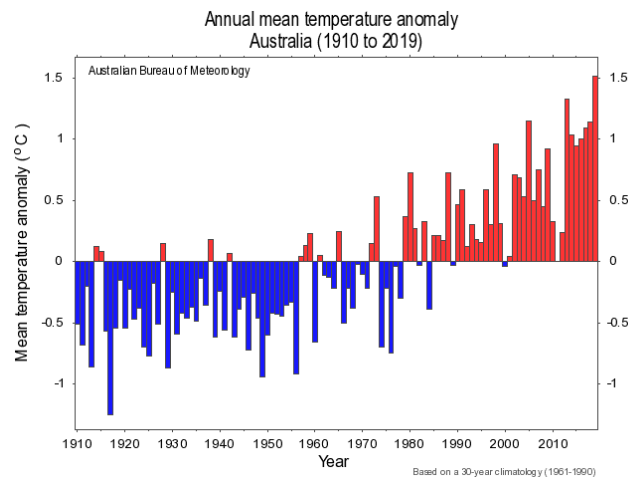


Figure 1.1: Data produced by the Bureau of Meteorology shows a warming of 1.5 degrees since 1950 (of Meteorology n.d.).

(Jolly, Cochrane, Freeborn, Holden, Brown, Williamson & Bowman 2015) validate this further, demonstrating global fire weather seasons have increased in length by 18.7% from 1979 to 2013.

To understand the cause of injuries involving hospitalisation, research was undertaken using media reporting from 2010 to 2020. The reported cause of volunteer firefighter fatalities in this time period is listed below. To gain a more holistic picture the search was not restricted to NSW volunteer firefighters but volunteers from every state and territory.

2012

In 2012, a Western Australian (WA) woman was killed when a firestorm engulfed her fire truck. The coroners report drew attention to the failings of the bushfire control officer to communicate to firefighters of a wind change. The report also found that a lack of vehicle protection and proper training for personnel also contributed to the women's death. However, the main conclusion was the many opportunities missed prior to the event for staff, including control officers to assess critical information. If such information had not been missed and appropriate action enforced, the fatality could have been avoided (Gubana & Southern 2017).

2013

In 2013, two Victorian firefighters were killed while fighting the Harrietville bushfire. The pair were working on the fire ground when a tree fell on their vehicle. The coroner found there was sufficient information available for incident control centre staff to act but 'not one person was in possession of all the fragments.' *'In hindsight, I find the system failed to ensure all available information was collated and considered as a whole, by ground and operations managers'* (Longbottom 2015).

2014

A South Australian (SA) volunteer firefighter was killed when standing behind a utility. The utility vehicle was struck by a fire truck while crews were fighting a blaze in the south east of the state. CFS Chief officer at the time Greg Nettleton, said the accident occurred in a *'low visibility situation where there was smoke around the area'* (*Second firefighter dies within weeks in SA* 2017). In a completely separate incident, a firefighter suffered burns to 70-90% of his body after falling from his truck.

2019

In a 2019 blaze, 2 NSW RFS volunteers from the Horsley Park brigade were in a truck convoy near the town of Buxton late on a Thursday afternoon when a tree fell into their path. With smoke so thick they could barely see 50 metres in front of them they manoeuvred causing the vehicle to roll off the road (Press 2019).

2020

In 2020, a Victorian volunteer firefighter was killed. The coroners report for the tragic event is yet to be completed but the death was believed to be caused by a falling tree (*'Much-loved' firefighter and father of two killed working on Victorian blaze* 2020).

For the period of 2013-2018 other volunteer firefighters tragically lost their lives while on the fire ground. However, these incidents were caused by cardiac arrest or other medical issues and could not have been foreseen or avoided by any kind of engineering control.

1.3 The Problem

During a bush fire, firefighters often operate in low visibility, high-temperature conditions while under extreme stress. With little information to rely on in a rapidly changing situation, firefighters often become disorientated, putting themselves and their crew at risk. Research has shown that in a high-stress fire environment, commanders and decision-makers often rely on past experience and instinct. For example, a crew rapidly trying to escape an approaching firestorm takes appropriate action based on the wind speed and direction, possible escape routes, and the environmental and road conditions at the time. When the only option is to drive through dangerous smoke-filled conditions, drivers are completely reliant on their vision to keep them safe and avoid an accident. Most commonly, accidents are caused by falling debris, trees, or other vehicles on the road. With little to no visibility, response time to see and react to such objects in such a heavy vehicle is often late, often resulting in a vehicle roll-over.

1.4 Research Aims & Objectives

The aim of this research is to select and evaluate a sensing system that can provide firefighters with real-time information that will improve situational awareness and safety in a bush fire situation. To achieve this aim, the project will be separated into individual objectives. These include:

1. Determine the most appropriate sensing technology to improve situational awareness for firefighting vehicles.
2. Evaluate the sensor's performance, with a specific focus on the risks associated with a fire environment. This includes:
 - Determine the maximum detectable range and range accuracy. ie at what range can object be detected and tracked.
 - Determine the peripheral capabilities of the sensing system
 - Determine the sensing characteristics of commonly found objects in a fire environment that pose a high risk to fire fighters
 - Validate the experimental results against the theoretical performance.

The increasing severity and bushfire occurrence in Australia demands a broader response and poses a greater risk to firefighters. This project investigates if new and existing technology can increase situational awareness of firefighters in high-stress situations with little visibility. The work will be fundamental to understand sensor capability and inform the future direction of a deployable system.

Chapter 2

Literature Review

2.1 Chapter Overview

This chapter aims to research and compile current knowledge in the space of firefighter situational awareness, with a specific focus on sensor technologies and information analysis. It begins with a brief introduction to situational awareness for firefighters and standard practice, a basic examination of various sensor technologies and their performance in smoke environments, and how sensor fusion methods can enhance situational awareness. The focus will then turn to millimetre wave sensing technology, including the relevant theory of object range and angular estimation using millimetre FMCW radar. Finally, radar cross section (RCS) will be introduced and its importance to radar design in the context of fire fighting situational awareness.

2.2 Fundamentals of Situational Awareness in a Fire Environment

'When firefighters don't know the language of fire behaviour, injuries and fatalities result' (Altman 2012). A deep understanding of fire behaviour is critical to situational awareness in a fire environment. Many firefighters have been seriously injured or killed by a lack of situational awareness caused by insufficient knowledge of fire behaviour. Without such an understanding, poor or inaccurate decision making at critical moments is highly likely,

often resulting in injury or death. (Klein, Calderwood & Clinton-Cirocco 1986).

Research has been undertaken in this space to understand methods commanders use in assessing a situation when making critical decisions at the scene of a fire. (Klein et al. 1986) investigated an interview method for obtaining a retrospective protocol of decisions made by fire ground command. Each decision was probed to determine:

1. *What cues and knowledge were considered when making a decision.*
2. *What other options were available.*
3. *How the chosen option was selected.*
4. *How much time was taken in making the decision.*
5. *What level of experience was required to make the decision.*
6. *What kind of critical cues and knowledge were missing*(Klein et al. 1986).

Results showed almost all decisions were made in less than one minute. This supports the most striking conclusion; rarely did any of the commanders attempt to compare or evaluate alternative options. In only 19% of cases, an alternative course of action was considered. Due to critical time pressures, decisions were made based on the commanders experience, drawing direct comparison from a previous incident and applying that knowledge to the current scenario.

2.3 Basic Examination of Sensor Technologies to Improve Situational Awareness in a Fire Environment

The rapidly evolving pace of a fire situation requires fast, accurate and reliable information in real time. As a result, sensor systems have traditionally not been utilised in front line fire fighting. Firefighting techniques and methods have gradually developed after multiple catastrophic fire seasons and this working knowledge has been the basis for improvement in practices. However, technology in Australian firefighting vehicles is gradually being upgraded to improve information gathering on the fire ground. With emerging new sensor technologies, the ability to provide accurate and reliable information in real time is now a possibility.

Generally, the most common sensor utilised in a fire situation is infrared (IR) thermal imaging. Fire research using portable IR imaging systems started in the late 1970's with an IR imaging system developed by Maxwell (1971). The aim was to observe forest fire behaviour through smoke to increase decision making ability. The system resulted in a significant improvement in observing and determining fire behaviour over what was standard at the time. IR imaging cameras underwent significant development over the following decades, by the late 2000's cameras had become highly advanced, enabling building fault detection or aircraft structure analysis. In these cases, detailed performance metrics are available, however, they fail to consider the harsh conditions of a bush fire. Amon, Hamins, Bryner & Rowe (2008) aimed to develop performance metrics that would provide IR camera manufacturers information to improve imaging performance. Several large scale experiments were performed in a variety of scenarios including with water vapour, dust and dense smoke. It was discovered that imaging needs are dependant on fire properties and the users activity. A common challenge observed was issues with dynamic range, resulting in insufficiently resolved features. In harsher conditions, the image saturates completely, therefore providing no useful information.

With sensor technology rapidly developing, firefighting organisations and researchers are investigating how they can be implemented to improve performance and safety. In addition to IR cameras, sensor technologies being considered as viable options include:

- Single echo light detection and ranging (LiDAR)
- Multi-echo LiDAR
- Sonar (Sound navigation and ranging)
- Night vision
- Standard cameras
- Radar

Researchers from Virginia Tech conducted an experimental study to quantify the listed sensors' performance in a fire smoke environment. Large scale experiments involved a fire and smoke filled hallway, where the visibility of the environment was monitored using a red HeNe laser. *Each of the sensors was evaluated for its ability to see through two different extremes of smoke; dense, low temperature smoke and light, high temperature*

smoke (Starr & Lattimer 2014). A summary of the results is shown in table 2.1. This includes the attenuation characteristics of each sensor within the 2 environments and visibility at which the sensor completely fails.

Table 2.1: Summary of sensor performance to see through two extremes of smoke. (Starr & Lattimer 2014)

A Comparison of Sensor Performance in a Fire Smoke Environment		
Sensor	Dense smoke, low temperature	Light smoke, high temperature
LIDAR Sensors	Attenuation at 4m visibility; failure at 1m visibility	No Effect
Visual Camera	Attenuation at 8m visibility; failure at 1m visibility	No effect
Kinect Depth Sensor	Poor results even with >8m visibility(combination of particle blocking and light saturation from fire)	Sensor Saturated with light for entire test
Night Vision	Failure at 4m Visibility	Sensor flooded saturated with light for entire test
Thermal Camera	No effect	No effect
Radar	No effect	No effect

The results show, thermal infrared cameras operating in the range of $7\mu\text{m}$ to $15\mu\text{m}$ and radars that operate at a wave length of approximately 11.5mm, perform well at seeing through dense smoke (Starr & Lattimer 2014). Visual cameras, LIDAR, night vision and the Kinect Depth Sensor all performed poorly in dense thick smoke, none of these sensors were found to be reliable when visibility was less than 4m. This is shown more clearly in figure 2.1, a target was setup in a room a distance of 1.8m from the instrument, the results show attenuation due to dense smoke starts to effect both LIDAR and colour cameras at a visibility of approximately 5m. Radar and Sonar reflections are not attenuated in dense smoke, even at the minimum testing visibility, one meter.

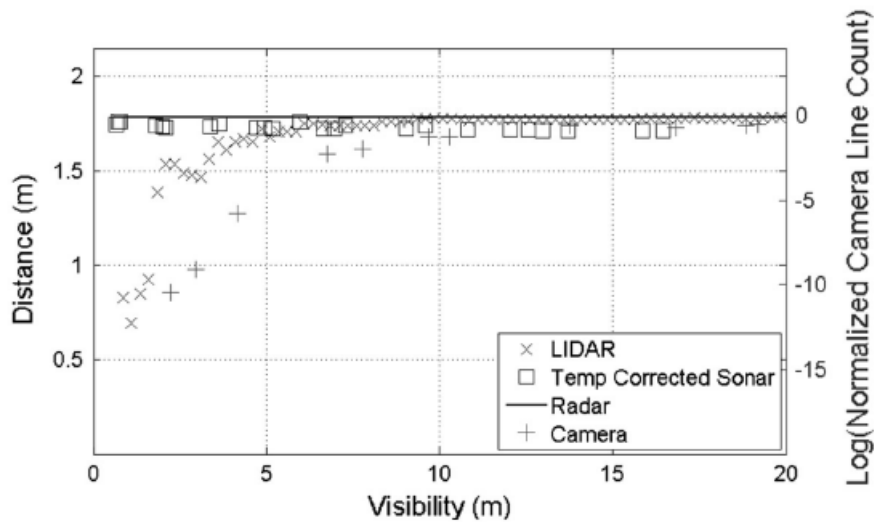


Figure 2.1: With a target object at 1.8m, data points display the attenuation due to smoke of the 4 selected sensors (Starr & Lattimer 2014).

From this result we conclude that millimetre wave (mm-wave) radar is one possible option to accurately measure range in smoke filled environments. Further work has been conducted using the mm-wave radar to provide more spatial resolution in a smoke filled space. Omine et al. (2004) performed experiments to understand signal return intensity for various objects. A visual representation of this can be seen in a point cloud plot in figure 2.2. This further shows mm-wave radar as a high accuracy, high fidelity sensor that is capable of providing spatially resolved information. This work is useful as it provides

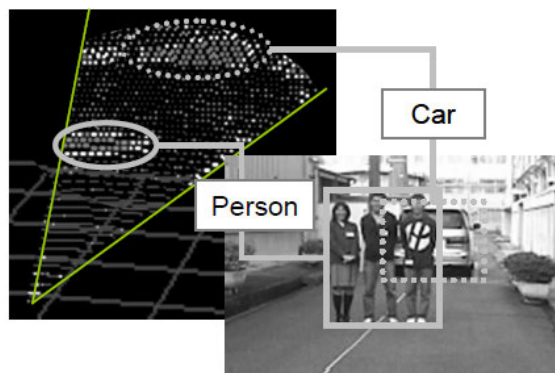


Figure 2.2: To identify objects the radar profile takes into account signal intensity. The signal intensity is dependant on the shape size and material properties of the reflected object (Omine et al. 2004)

not only range information but spatial resolution. Further, Clark & Dissanayake (1999) conducted vehicle automation experiments using mm-wave radar in an outdoor environment. The experimental setup investigates using the polarisation of returned radar signals

to identify natural environmental or man-made features to address the problem of simultaneous localisation while driving through an environment. Results show metallic objects with corners, such as those found in industrial environments, must be present for the system to detect and adjust position accurately. The ability to identify the exact nature of an obstacle or hazard in a high stress, smoke-filled environment is invaluable information for firefighting, making these results highly applicable to the problem of situational awareness on the fire ground.

2.4 Sensor Fusion for Increased Situational Awareness

As shown, mm-wave radar is capable of producing high fidelity information in a fire smoke environment. However, the nature of an object is difficult to determine solely from radar information. Generally, in high-stress fire environments, visual sensory information is relied on to identify hazards. This specific feature is relied upon for situational awareness and is the major failing when relying solely on mm-wave radar.

2.4.1 Fusion of mm-Wave Radar with Machine Vision

In the context of situational awareness for fire fighting, fusing mm-wave radar sensing with machine vision is a promising technology. Combining the two sensors in a single platform addresses the individual deficiencies of each sensor. Radar sensing is not dependant on weather or lighting conditions and has high range accuracy, although, angular accuracy is poor. In contrast, camera sensing techniques have poor ranging capability, are highly susceptible to lighting and environmental conditions but have quality angular sensitivity and can obtain detailed object information such as pattern and shape (Kim, Kim, Lee & Park 2017).

The potential of this technology is presented in an experimental study conducted by Kim, Starr & Lattimer (2015). Object detection using a fused stereo infrared vision and radar sensing platform in a smoke environment was investigated. Sensors were tested individually and compared with experiments conducted using the fused platform under similar conditions. Results show the stereo IR system alone detected 3 of the 4 objects, also detecting 2 ghost objects due to the stereo IR mismatch. The radar system detected all 4 objects but the radar also penetrated the rear wall of the hallway, detecting 3 objects

not relevant to the study. *With the fusion of two sensors the ghost objects from the stereo IR were eliminated and objects identified using the radar outside the field of view were removed* (Kim et al. 2015). In addition, the fusion of sensors reduced the distance error from 1-19% to 1-2%.

The significance of this result in a bush fire environment is unknown. If mm-wave sensing as a singular device does not provide adequate information to improve situational awareness, a combination of mm-wave and stereo IR sensing looks to be a promising option.

2.5 Fundamentals of Millimetre FMCW Sensing

The advancement of self driving vehicles in the automotive industry, in part, is due to the miniaturisation and development of FMCW radar sensors. FMCW radar is now affordable, compact and capable of measuring many parameters, including; range, velocity, bearing, elevation and doppler shift. This is what differentiates FMCW from conventional CW (Continuous Wave) radar systems. The major advancement being the ability to accurately determine target range, *CW radar cannot determine target range because it lacks the timing mark necessary to allow the system to time accurately the transmit and receive cycle to convert this into range.* (Faulconbridge 2002). As with all radars, energy travelling towards an object is reflected and travels back towards the receiving antenna. This takes a finite time which provides a measure of the objects range. To apply this to FMCW radar, figure 2.3 shows the transmitted and received signal in the time domain.

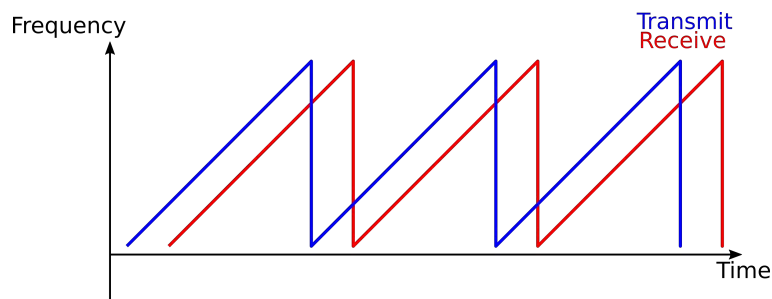


Figure 2.3: Transmit and receive wave forms for a FMCW radar with a stationary target using a saw-tooth wave.

FMCW radars commonly use a form of linear frequency modulation such as a saw-tooth or triangular wave. The fundamental theory of FMCW and how range is obtained is best explained by Constapel et al. (2019). The continuous transmission is separated into packets often named loops, each loop consisting of a number of linearly frequency modulated fragments, called chirps which oscillates to the bandwidth B over time period T_{chirp} with slope m as shown in figure 2.4. The transmitted chirp is reflected off the target and a time delay version of the signal is received by the radars antenna denoted T_d . The time delay of the chirp corresponds to the distance to target but it cannot be measured directly. Instead, the received signal is mixed and therefore multiplied with the transmission signal, yielding the frequency difference f_B . Utilising a fast Fourier transform (FFT), the frequency difference f_B over time represents a frequency tone which is characterised as the *beat frequency*. This peak frequency corresponds to the distance to target at a maximum range R_{max} .

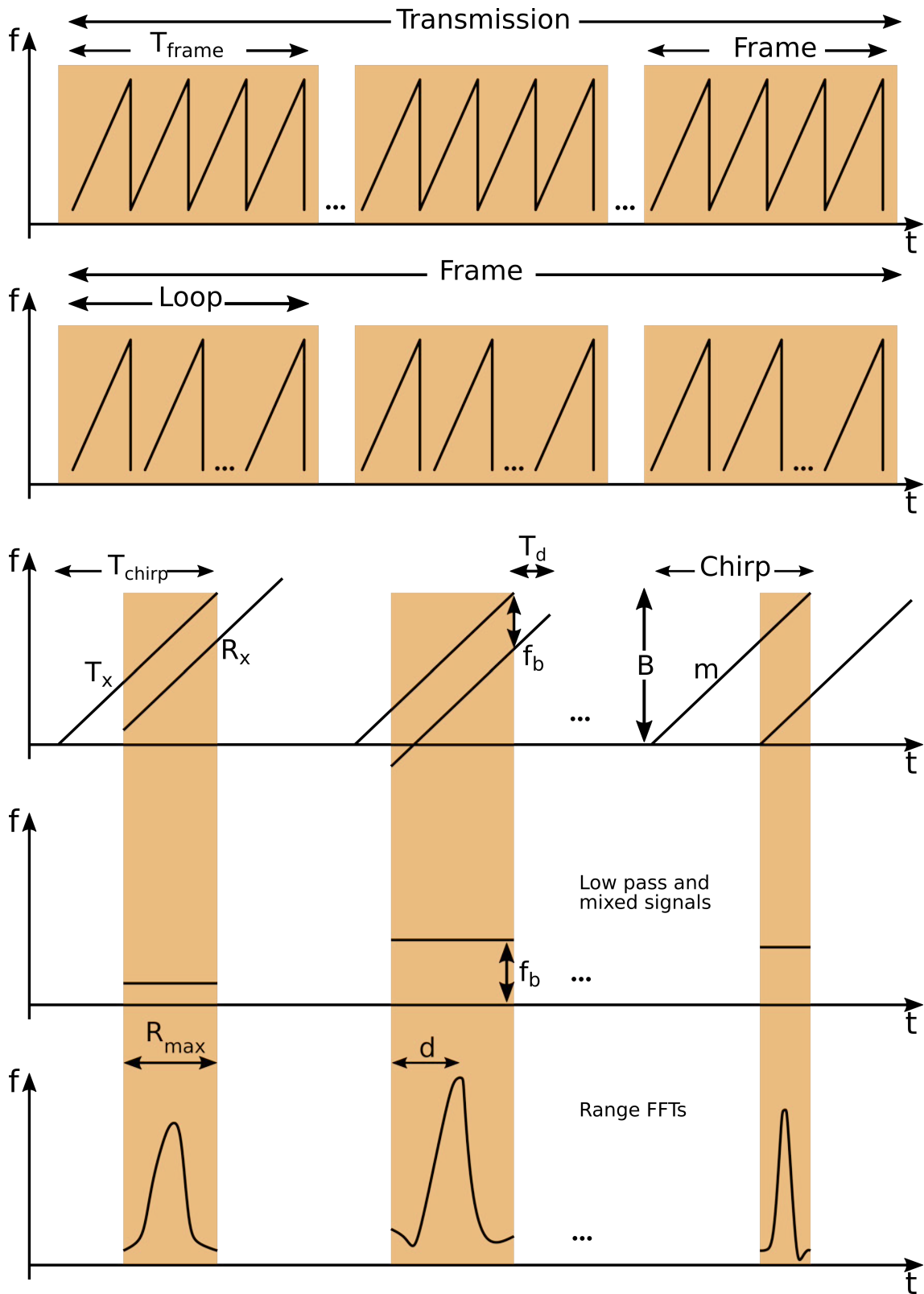


Figure 2.4: The relationship between frames, loops and chirps Constapel et al. (2019)

2.6 FMCW Radar Range & Angle Measurements

Radar systems transmit electromagnetic waves that objects in their path then reflect. By transmitting and capturing the reflected signal, mm-wave FMCW radar can determine the objects' range, velocity, and angle. A significant advantage of short wavelength, mm-wave sensing is high range accuracy. Millimetre-wave operating at 76-81 GHz with a corresponding wavelength of approximately 4mm, can detect movements as small as a fraction of a millimetre or an objects range within a similar tolerance.

2.6.1 Radar Range Measurement

The range, range accuracy and range resolution are all heavily dependant on chirp parameters selected. Figure 2.5 shows chirp frequency as a function of time where the start frequency is represented by (f_c) bandwidth (B) and duration (T_c). The slope of the chirp (S) captures the rate of change of the frequency (Faulconbridge 2002). In the example provided in figure 2.5, $f_c = 77\text{GHz}$, $B = 4\text{GHz}$, $T_c = 40\mu\text{s}$ and $S = 100\text{MHz}/\mu\text{s}$.

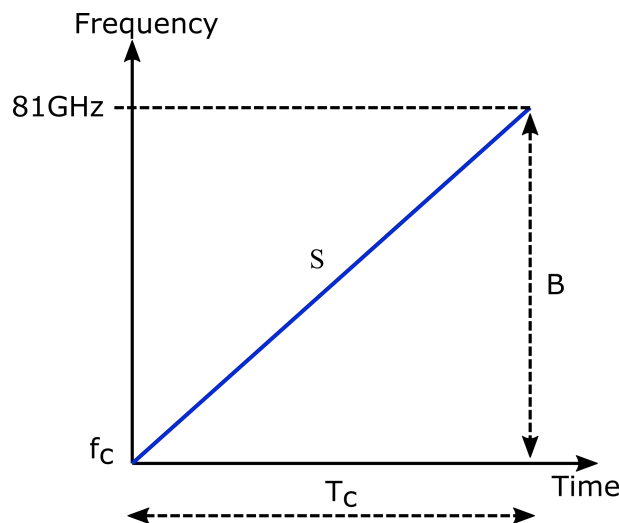


Figure 2.5: Chirp signal, with frequency as a function of time (Faulconbridge 2002)

As shown in figure 2.4 after mixing, beat frequency is proportional to the frequency difference f_b , therefore any non linearity in transmission T_x will impact range accuracy. Maintaining linearity is a key challenge with FMCW radar systems, any change in slope of transmission will influence beat frequency, resulting in poor range resolution.

Unlike chirp linearity, which is predominately determined in hardware, transmission time T_{chirp} is entirely within the control of radar operators and will determine the maximum detectable range. Transmission time and its dependant properties need to be carefully selected to suit the application, including the maximum detectable range of specific radar cross sections. The importance of this is shown in figure 2.6. Shown in black is a transmission signal along with 3 reflected signals in blue, red and green. Labels f1-f3 reflect the beat frequencies of the corresponding transmission and return frequencies. The beat frequency f1, can be extracted and quantified using the process described above. The maxima of the red curve represents a target that is further away and again the beat frequency can be extracted and quantified. Naturally, f2 is larger than f1 as the target is located further away from the radar. The target represented by the maxima of the green curve is further away still, only this time the beat frequency starts to become ambiguous. Note beat frequency f3 and f2 are the same, even though the reflections are clearly at different ranges. This beat frequency (f3) and the subsequent range calculation will return an incorrect result (Faulconbridge 2002). For this reason, chirp transmission time and the resultant slope is critical when determining maximum detectable range. Range ambiguity is related to the modulation rate of the FMCW radar. To calculate the maximum unambiguous range of the radar in meters:

$$R_{unambiguous} = \frac{c}{2f_m} \quad (2.1)$$

where:

$R_{unambiguous}$ = Maximum unambiguous range in meters

c = Speed of light ($3 \times 10^8 \text{ ms}^{-1}$)

f_m = Modulation rate in Hertz

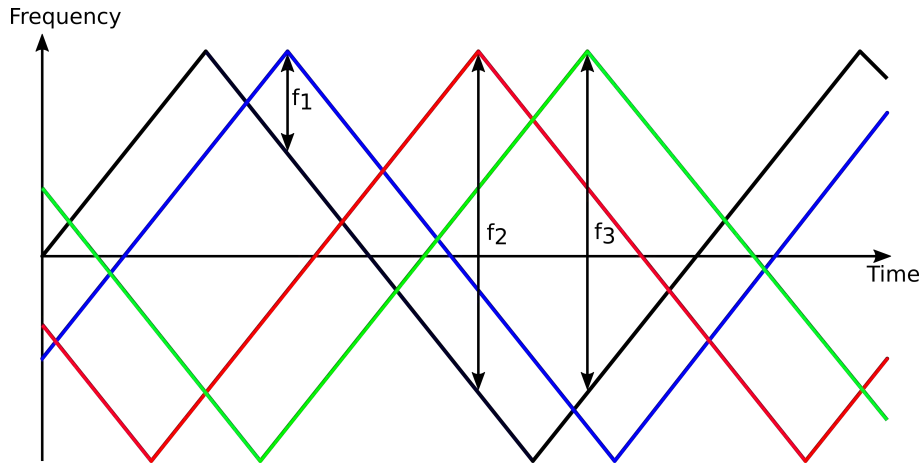


Figure 2.6: FMCW Range Ambiguity. Reproduced from (Faulconbridge 2002)

In addition to knowledge of chirp parameters and limitations, controlled in software, the radar range equation (RRE) is a valuable expression for engineers and radar operators. The range equation relates the range performance to essential hardware components and their characteristics. These include:

- Transmitter (transmitted energy);
- Receiver (minimum detectable signal strength)
- Antenna (gain and beam width)
- Target (radar cross section [RCS])

In the context of this work, transmitter power and antenna gain are fixed parameters. Traditionally these parameters are variable and can be adjusted to influence radar performance. Radar cross section is an important parameter in radar system design, as it is a measure of a targets ability to reflect the intercepted signal back toward the radar receiver. Results presented in this work will focus on this parameter and its relevance to the problem of situational awareness for fire fighting. The RRE comes in many variations, the simplest and most useful is shown in equation 2.2. This expression states the received power (P_r) in watts from a reflected object is equal to:

$$P_r = \frac{P_t G_t G_r \lambda^2 \sigma}{(4\pi)^3 R^4} \quad (2.2)$$

where:

P_t = Transmitted power (W)

G_t & G_r = Transmitter and receiver gain respectively (as a ratio)

λ = Wavelength (m)

σ = RCS (m^2)

R = Distance to target (m)

This equation is often used by radar design engineers to specify hardware components and characteristics in order to detect, track and identify specific objects at a known range. Additionally, it can be used to predict a range for a given RCS if other parameters have been set.

2.6.2 Radar Angle Detection

Using multiple transmit and receive antennas it is possible to *estimate* the angle of a reflected signal, and therefore the angle to the target. A change in the distance to a target results in a phase change in the peak of the range-FFT (*IWR1443BOOST Evaluation Module mm-Wave Sensing Solution* 2018). This same theory, along with at least two receive antennas, is used to perform angular estimation. The differential distance of the object to each antenna results in a change in the FFT peak. This phase change is an estimate of the angle of arrival (AoA).

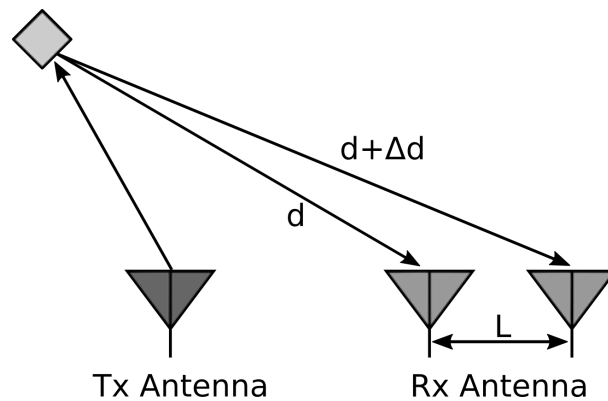


Figure 2.7: Estimating AoA with two antennas. Reproduced from (Rao, S 2017)

Using the configuration shown in figure 2.7, the phase change is derived as:

$$\Delta\phi = \frac{2\pi\Delta d}{\lambda} \quad (2.3)$$

Utilising basic trigonometry shows that $\Delta d = l\sin(\theta)$ where l is the distance between antennas (*IWR1443BOOST Evaluation Module mm-Wave Sensing Solution* 2018). Therefore the the AoA (θ) can be evaluated with equation 2.4:

$$\theta = \sin^{-1}\left(\frac{\lambda\Delta\phi}{2\pi l}\right) \quad (2.4)$$

2.6.3 Maximum Angular Field of View

It should be noted, $\Delta\phi$ depends on $\sin(\theta)$. This is called a non linear dependency. $\sin(\theta)$ is approximated with a linear function only when θ has a small value: $\sin(\theta) \sim \theta$ (Rao, S 2017). Therefore, estimation accuracy depends on the AoA and is more accurate when θ is close to zero. Theoretically, with a spacing between the two antennas of $l = \lambda/2$ results in a maximum angular field of ± 90 deg (Rao, S 2017). However, reliable measurements will only be achieved at an angle significantly smaller.

2.7 Radar Cross Section Measurements

Radar cross section, σ as shown in equation 2.2, is one of the most critical parameters in radar system design. The RCS of the target is outside the control of radar designers or operators, but can be estimated and allowed for. RCS is measured in m^2 , fundamentally it is a measurement of how well a target reflects intercepted energy back to the receive antenna. Mathematically, RCS can be defined as:

$$\sigma = \frac{4\pi R^2 S_r}{S_t} \quad (2.5)$$

where:

$\sigma = \text{RCS } (m^2)$ $R = \text{Target range } (m)$

$S_r = \text{Scattered power density } (W/m^2)$

$S_i = \text{Power density intercepted by the target } (W/m^2)$

As shown, RCS (σm^2) is not the same as physical cross section. Sometimes the physical area of the target is larger than the RCS due to scattering and absorbent effects caused by the targets shape and material properties. Other times, a small object can have a large radar cross section, contradicting its physical size (Faulconbridge 2002). Due to the rapid uptake in mm-wave sensing technologies, specifically in the automotive and aviation industry, many common objects such as cars, pedestrians, trucks and aircraft have a well characterised RCS, An example of this is depicted in figure 2.8.

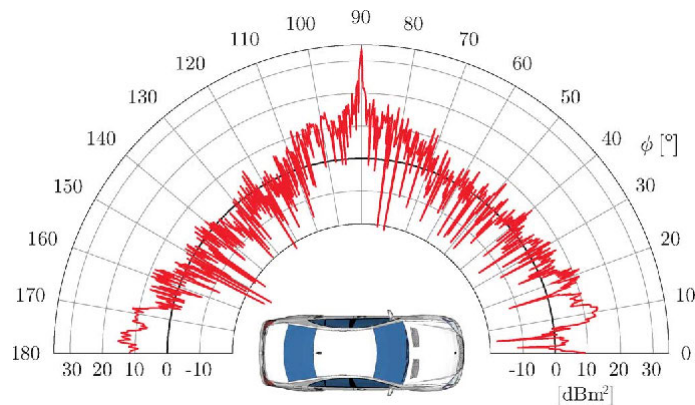


Figure 2.8: Radar return intensity of a typical car. (Buddendick & Eibert 2010)

(Bel Kamel, Peden & Pajusco 2017) focused on automotive radar target modelling and experimental verification in order to optimise detection systems. A 3D CAD model of a know vehicle geometry was discretised into small triangular sections in order to achieve an accurate estimation of scattering contribution for each section. To complement simulations, RCS experiments were conducted in a large open gymnasium over the 76-81 GHz frequency range. Radar intensity measurements were taken by manually moving the experimental setup in 2 degree increments. It was found that the maximum RCS of vehicles tested varied between 19-25 dBsm. Work more applicable to a fire environment using a similar methodology has been undertaken to understand RCS of more complex geometries such as trees (Mrdakovic, Olcan & Kolundzija 2015). Modelling performed at frequencies 0.2, 0.5 and 1.5 GHz demonstrated the proposed approach can be used to

calculate stochastic RCS of real size trees in the GHz range. Further, (Mougin, Lopes, Karam & Fung 1993) performed an experimental study to investigate the relationship between various trees and X-Band radar signal. For a single tree the RCS is measured as a function of scatter. Results show the tree's architecture has a large influence on the RCS, with leafy branches the primary source of scattering. Importantly, the RCS in the vertical orientation is significantly different to the horizontal. This is attributed to the relatively simple structure at the top of the tree, compared to the complicated structure lower on the trunk of the tree.

Further work understanding mm-wave backscatter from deciduous trees or RCS of Australian forest fire ash has been completed by various authors. This work is notable as it is fire related. However, it specifically addresses fire detection methods, not obstacle or object detection in a fire environment (Baum, Thompson & Ghorbani 2011).

2.8 Conclusions

This chapter reviewed available literature in the field of firefighter situational awareness and how it can be improved. Specifically it reviewed 5 key areas:

1. Information and decision making processes utilised by firefighting commanders in order to make accurate and timely decisions.
2. Sensor technologies that are applicable to situational awareness in a fire smoke environment.
3. The effect sensor fusion has on reliability and accuracy of information.
4. Fundamental theory of FMCW radar, the importance of chirp parameters and the range equation to determine maximum detectable range, and how angular estimation is performed.
5. The importance of RCS and previous work focussing on this parameter within the context of firefighting.

From the literature, it is obvious that firefighting commanders in a bush fire scenario make difficult decisions on the fly with limited information. A sensor system that can provide

reliable timely, accurate information that is insensitive to environmental conditions will improve decision making. Multiple sensing technologies look promising for fire fighting applications, this research will focus on automotive mm-wave radar sensing technology. This technology is affordable, compact, highly accurate and versatile. The sensing system can be programmed for a specific application, ie detect a specific object at a known range. Based on this, a radar chirp parameter suitable for fire fighting vehicles will be selected and characterised. This result produces more sensor focused aims and objectives. These include:

- Determine the maximum detectable range of various cross sections applicable to a bush fire environment.
- Evaluate the maximum angle an object can be detected off boresight (angle of maximum return signal, typically 90°)
- What is the radar cross section of a typical gum tree in the 76-77 GHz frequency range, and
- What effect does the orientation of the gum tree (standing or fallen) have on RCS.
- Finally, validate the results against common radar design tools to verify if traditional calculations can be utilised for determining maximum detectable range of any RCS.

Chapter 3

Methodology

This section outlines the methodology used to evaluate the mm-wave sensor for firefighting situational awareness. Specifically, an experimental study will be completed to identify the maximum detectable range, angular resolution and capability of mm-wave sensor information in identifying objects such as trees.

3.1 Radar Sensor Selection

Over the years, the advancement of 77GHz RF design with integrated digital CMOS technology and packaging, has enabled low cost on chip radar and antenna systems (Großwindhager, B 2019). The radar selected for this research is one such product, the Texas Instruments IWR1443 Boost FMCW mm-wave radar. IWR1443 boost is an evaluation module to get started with millimeter wave radar sensing. The boost module is approximately 65x85mm in size with printed onboard antennas. These chips are relatively new, until recently were difficult to obtain in Australia. Texas Instruments produce a family of these radar modules aimed at various industries. Also available to select from is the AWR1642 boost, aimed at the automotive sector. Functionally there is no difference between AWR (Automotive) and IWR (Industrial) series sensors. The primary difference is AWRxxxx series supports a wider temperature range, -40 - 125C. The IWR supports -40 - 105C, and AWRxxxx devices are automotive qualified, meeting specific automotive and radiation standards (*IWR1443BOOST Evaluation Module mm-Wave Sensing Solution* 2018). Notable features of the IWR1443 include:



Figure 3.1: Texas Instruments IWR1443 Boost mm-wave FMCW Radar Sensor (*IWR1443BOOST Evaluation Module mm-Wave Sensing Solution* 2018)

- 3 Transmit antenna, 4 Receiver antenna
- Capable of customising antenna setup
- Transmit power – 12 dB
- Antenna peak gain - 10.5 dBi
- Simple user friendly out-of-box software available
- Highly affordable at around \$700 AUD

Texas Instruments provides a comprehensive library of software to operate and work with the IWR1443. Measurements shown in this dissertation were undertaken using a 3rd party robot operating system (ROS) package as discussed in section 3.2.1 - Data Collection using ROS. However, to operate this ROS package requires the latest software image. This can be found in TI's software development kit (SDK) available on TI's website. The image used in this work was the `xwr14xx_mmw_demo.bin` image in SDK version 2.01.00.04 under `...\packages\ti\demo\xwr14xx\mmw`. To load the image onto the device, the stand alone or online TI Uniflash tool is required. To perform this task, detailed instructions are available in the *SDK Users Guide*.

3.2 Chirp Parameters

As outlined in section 2.6.1 - Radar Range Measurements, chirp parameters of FMCW sensors are customisable to optimise performance and reliability, taking into account the

physical characteristics of the environment. These parameters essentially act as tuning knobs for developers and researchers. Depending on the application, users prioritise certain metrics (Großwindhager, B 2019). Typically these metrics are:

- **Best Range Resolution** - Parameters are selected to ensure optimum performance in a static or slowly changing environment, where highly accurate range measurements to the object(s) is required. This is typically used in indoor mapping, gesture detection or small object detection.
- **Best Velocity Resolution** - The aim of this setup is to optimise for velocity resolution. It is suitable for detecting and tracking highly dynamic objects. Typically, it is used in application involving UAV's or robotic systems.
- **Best Range** - This setup optimises for maximum possible range. Hence, the aim is to maximise the maximum detectable range while maintaining a reasonable range resolution. Typically, this configuration is used in outdoor environments, such as motor vehicle automation.

For this work, chirp parameters were selected to optimise *Best Range* at the frequency range 76-77 GHz. To select these parameters, TI has a number of online tools available. The Demo Visualizer is an out of box online tool that allows you to upload, save and visualise radar information. Within the demo visualiser you can select and export chirp configurations to suit the users application, this information is exported as a `cfg` file. The Sensing Estimator is an online tool, providing a depth of adjustment to optimise chirp configurations. The sensing estimator provides more capability, unfortunately, it only exports the chirp configuration in `.JSON` format. The IWR1443 will only accept the chirp parameters in `.cfg` format. Transferring between JSON and `cfg` is not trivial, for this reason, the demo visualiser was used to generate chirp parameters to detect targets at a maximum detectable range of 50m. Chirp parameters used and there corresponding meaning are shown in table 3.1 and figure 3.2.

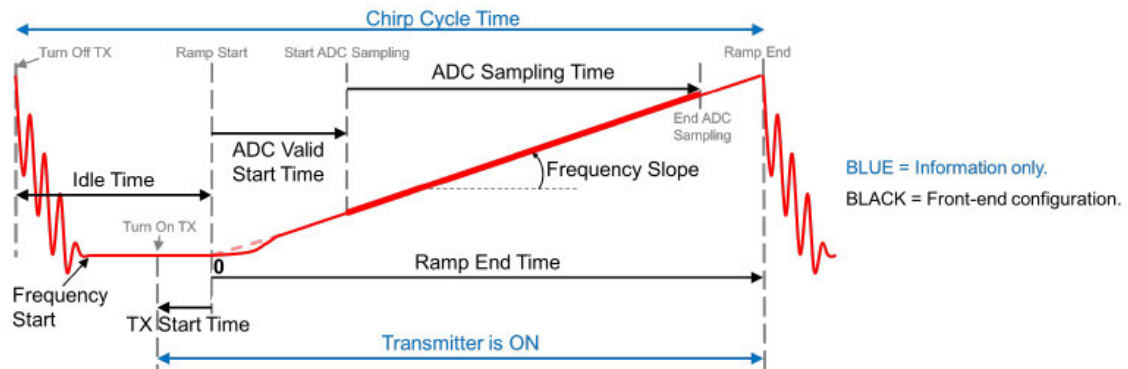


Figure 3.2: Chirp parameter configuration for TI mm-wave devices (Texas Instruments 2018)

Table 3.1: Summary of chirp parameters, and resulting radar accuracy and resolution. Parameters were specified using TI's Demo Visualiser software.

IWR1443 Chirp configuration - 50m range	
Front end Configuration	
Idle Time	444 μ s
Frequency Start	76 GHz
Tx Start Time	1 μ s
ADC Valid Start Time	7.0 μ s
ADC Sampling Time	256
Frequency Slope	15 MHz/ μ s
Ramp End Time	48.98 μ s
Resulting parameters	
Number Tx	2 Antennas
Rx Gain	30 dB
Range Resolution	0.23439m
Max Doppler Velocity	1.989 m/s
Max Allowed Elevation	90deg
Max Allowed Azimuth	90deg
Max Range	50m

A critical parameter to this work not well discussed in TI's documentation is range detection threshold (RDT). All TI mm-wave sensors have onboard firmware that performs data processing of FFT information. *The employed firmware uses a cell averaging constant false alarm rate (CA-CFAR) to detect object in the field of view of the radar. The task of the algorithm is to determine the power threshold above which a received signal can be assumed to originate from a certain object* (Großwindhager, B 2019). If this threshold is set to high, less objects will be detected, however the number of false alarms detected will be lower. If the threshold is set to low, more objects will be detected, only at the cost of more possible false alarms. The 50 meter chirp configuration used has a 15dB RDT.

3.2.1 Data Collection using ROS (Robot Operating System)

A ROS package developed by TI software engineers, and customised by (Zhang 2019) was used to drive the mm-wave radar sensor. ROS is a Linux, package based middle ware for robotics applications. Using a package based framework allows software drivers, simulation tools and any third party code to seamlessly be shared and implemented into your working environment. The true power of ROS is the time and resources saved by gathering all the appropriate tools needed to develop projects. ROS is designed to be a loosely coupled system, each task is individually broken down into a single node. Nodes then communicate with one another, passing messages via channels called topics. Each node can send or receive data from other nodes using the publish or subscribe commands.

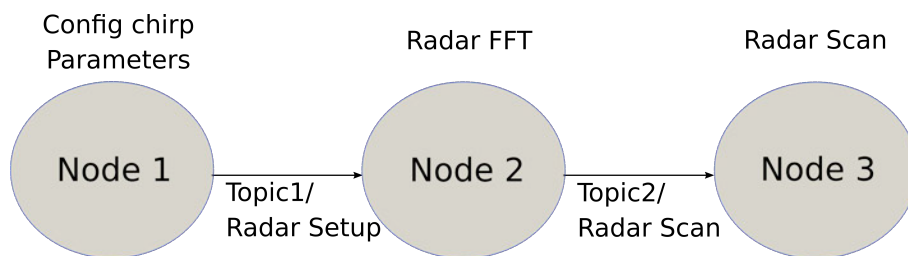


Figure 3.3: Basic Architecture of the ROS Environment

To save the data, users simply subscribes to the topic *Radar Scan* using the inbuilt ROS function, *rosvag record*. This merely taps into the data transmission between nodes 2 and 3 and saves what it sees to a rosvag file. This is done with one line of code on a Linux terminal - `rosvag record -o <file name> .../radar_scan`. The rosvag file is later converted to CSV format for data processing.

3.3 Triangular RCS Target

Six major factors influence RCS, including; size, shape and reflectivity of the object as well as the radars transmit frequency, signal polarisation and the angle to target. To evaluate the maximum detectable range and influence RCS has over this parameter, triangular corner reflectors of a known RCS were manufactured and tested. To achieve this, all possible parameters were fixed, only size is varied in order to changed the RCS. As RCS varies so greatly with these parameters, general figures were selected based on commonly used data from law enforcement radar systems. RCS is a critical parameter in identifying and tracking speeding vehicles (CopRadar 2018).

Expression 3.1 is used to determine the size of triangular corner reflectors.

$$\sigma = \frac{4\pi a^4}{3\lambda^2} \quad (3.1)$$

where;

$\sigma = \text{RCS } (m^2)$

$\lambda = \text{Wavelength (m)}$

$a = \text{the side length (m) of the 3 isosceles triangles, as shown in figure 4.2 (Tutorial 2020).}$

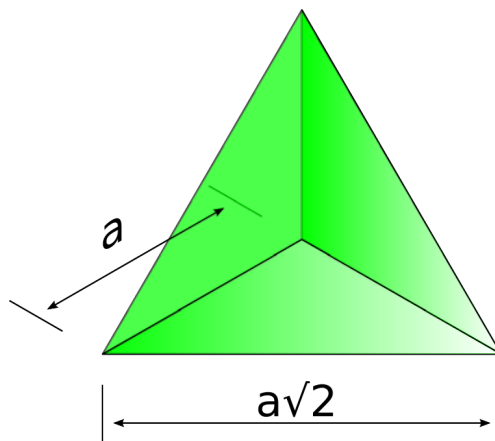


Figure 3.4: Triangular corner reflector. Reproduced from (Tutorial 2020)

Re-arranging this expression for a , lengths; a and $a\sqrt{2}$ were determined for the 4 RCS's selected; 400, 200, 120 and $60m^2$. These figures are shown in table 3.2.

Table 3.2: Tabulated triangular corner reflector calculations based on equation 3.1

Triangular Radar Cross Section Corner Reflectors				
Target Designation	Simulated Vehicle	RCS (m^2)	a (mm)	$a\sqrt{2}$ (mm)
T1	Large RV or Fire Truck	400	195.2	276
T2	Large Utility	200	164.2	232.2
T3	Large Car	120	144.5	204.3
T4	Mid-Size Car	60	121.5	171.8

To ensure consist signal scattering across all targets, corner reflectors were manufactured on a precision welding table, shown in figure 3.5. Triangular sections for each target were guillotined from a large sheet of polished stainless steel, corner reflectors were then welded together using a gas tungsten arc welding (GTAW) method.

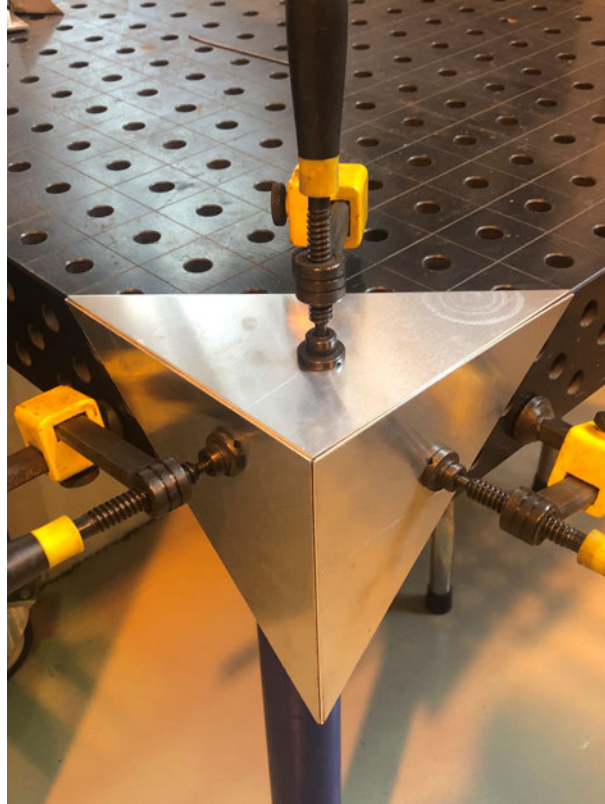


Figure 3.5: The fabrication of triangular corner reflectors was completed on a precision welding table using the GTAW method.

3.4 Maximum Detectable Range

Site selection is critical for determining maximum detectable range and angular resolution. Traditionally, experiments such as these are conducted in a large anechoic chamber. For these experiments, this type of facility is not feasible or available. To minimise back scatter and reflections from foreign objects, a large open area was required. The site shown in figure 3.6, located on a property in Wallaroo, is flat with no distinguishable objects within the expected range.



Figure 3.6: Site selection for maximum detectable range and angular resolution experiments

To evaluate maximum detectable range of RCS targets 1-4, the experimental setup shown in figure 3.7 is utilised. Each target is setup in a large open field on a threaded rod approximately 1200mm from the ground. A tape measure is run along the ground and radar measurements are taken in 5 meter increments a distance R from the target. The tripod housing the radar is adjusted at each increment until maximum intensity (radar bore sight) is found. The ros bag command (discussed in section 3.2.1) was then called and data was recorded for approximately twenty seconds. This process was repeated at each increment until a maximum distance is found. At maximum range, return intensity is equal to the range detection threshold. At this point no more samples are collected as previously discussed in subsection 3.2.

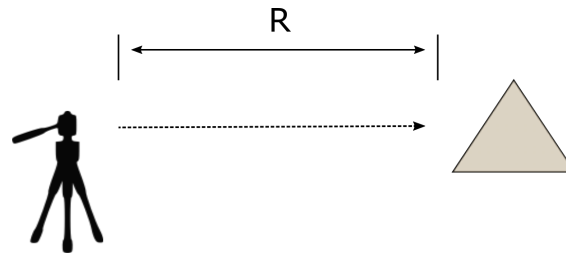


Figure 3.7: Experimental schematic for determining maximum detectable range

3.5 Peripheral Sensing Capabilities

Experiments to determine angular resolution are conducted in a similar manner to that shown above. The triangular reflectors are mounted on a threaded rod approximately 1200mm from the ground and 15 meters from the radar. Similarly, the radar is mounted on a threaded rod that is then clamped in a dividing head, this is shown in figure 3.8. Before clamping, the height of the radar is adjusted until bore sight is obtained. The radar is then rotated in one degree increments, at each increment the `ros bag` command is used and data is saved for approximately twenty seconds.



Figure 3.8: Beam width calibration

3.6 Radar Cross Section Measurements

Radar cross section measurements of organic materials, such as trees have not been well characterised at the higher frequency ranges. To perform these experiments, 2 large gum trees were selected as a test case. These trees are situated on reasonably level ground with no obstructions or other foreign objects within a detectable range. The setup used is similar to that shown in subsections 3.4 and 3.5. However, in this instance, the target (tree) is kept stationary and the radar is rotated around an arc circle of the object. An illustration of this is shown in figure 3.9. An arbitrary location, a distance of 15 meters from the tree is designated the starting point. Using simple trigonometry the arc circle is broken into 2 degree segments, these segments were marked on the ground with line marking paint. At each increment the radar is adjusted to bore sight before the ros bag function is again used to save sampled data over a twenty second time interval. A total of 91 measurements are taken from 0-180 degrees.

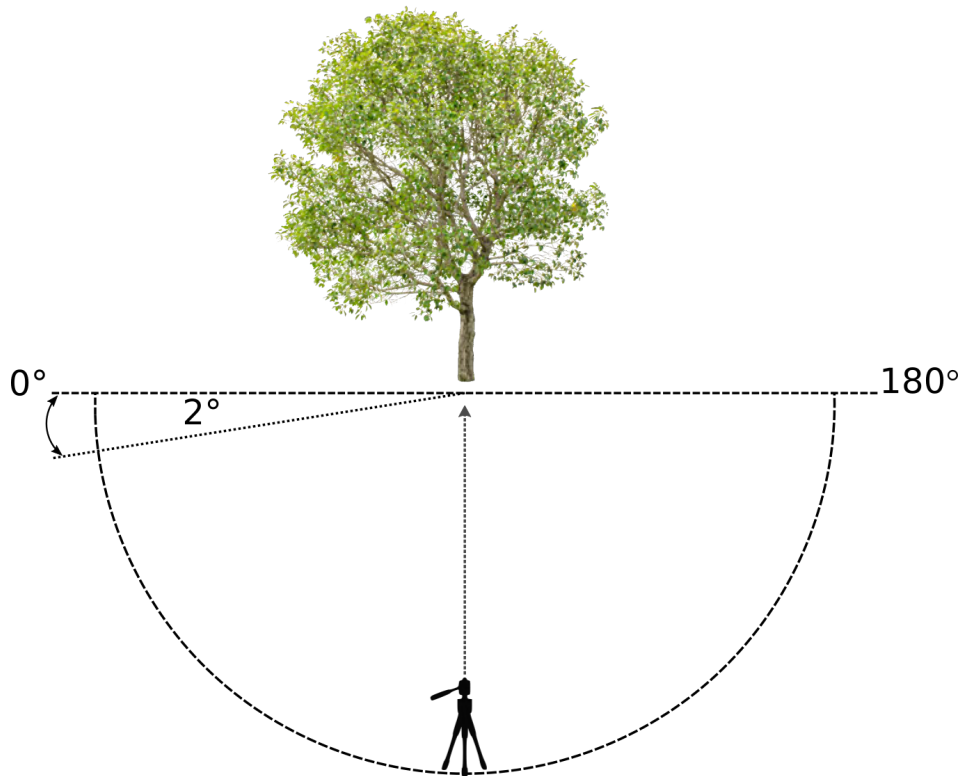


Figure 3.9: Radar cross section of various trees

3.7 Data Processing

As discussed in subsection 3.2.1, data is collected using the Linux based middle ware, ROS. Post processing the data involves converting ros bag data files into CSV format. This is achieved with open source code (Speal 2013) developed at McGill University - Space Mechatronics Laboratory. Once all files are in CSV format and named appropriately, data is ready for processing. Each file is labelled with the name of the experiment and distance to target. An example file name: `max_range_T1_{<Distance>}`.

Numerous Python scripts were written to process and analyse the results. Each script is different, however, the fundamental process does not change. The python snippet shown in appendix f analyses the data collected for the maximum detectable range of the corner reflector, T1. The only input required by the user is number of files recorded. First, variables are pre-allocated, a `for` loop then opens the first file (closest distance to target), saves the intensity or required data to a variable and calculates mean and standard deviation. Before repeating, distance to target is incremented. The loop then repeats, opening the next file in the directory. After processing and relevant fitting, a plot in the appropriate format is produced.

Chapter 4

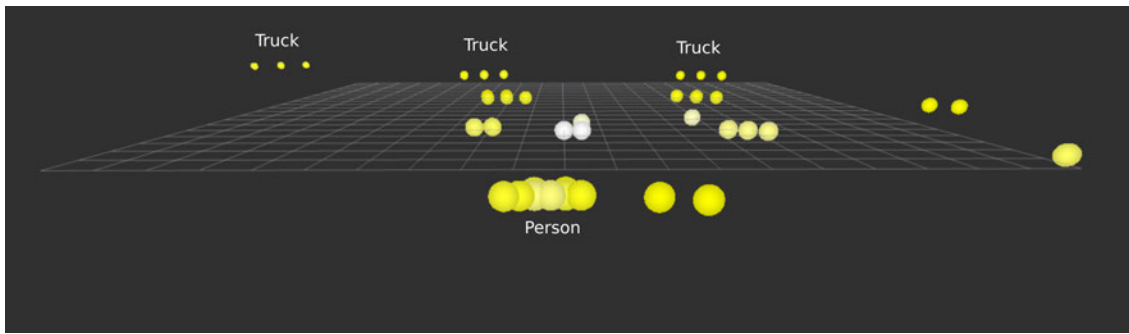
Results & Discussion

Numerous experiments were undertaken to evaluate maximum detectable range, peripheral capabilities, and radar cross section of typical objects found in a fire environment. Results presented in this chapter are those performed using the 50m range chirp parameters as outlined in subsection 3.2. Further results utilising a medium range parameter focusing on velocity resolution can be seen in appendix C and will be referred to throughout this chapter.

Firstly, results showing the maximum detectable range of various RCS corner reflectors will be presented. Further, the range accuracy will be quantified and discussed. This is followed by a discussion on the peripheral capabilities of the radar sensor, which is validated against measurements published by Texas Instruments. Radar cross section measurements taken of both a standing and fallen tree will be presented. Finally, results will be compared against the radar range equation in order to determine the practicality of utilising the RRE as a design tool for TI's FMCW radar platform.

4.1 Initial Testing

Initial testing was undertaken to understand the capabilities and limitations of the radar sensor. Measurement fidelity was evaluated by statically mounting the radar on a tripod and faced towards multiple heavy vehicles, approximately 15 meters from the instrument, as shown in figure 4.1(a). This figure and the corresponding photographic image of



(a) Point cloud plot of 3 trucks and a person



(b) Image showing the corresponding 3 trucks and a person

Figure 4.1: Radar data visualised

the scenario, shows objects such as trucks and people can be graphically visualised and spatially resolved in 3 dimensions. Each circle in 4.1(a) represents a reflection; the shade of yellow of each reflection is an indication of the reflected intensity. As shown, object range can be evaluated and the type of object can be inferred based from the signal return intensity and spread of reflections. However, a number of false detection's shown in a light shade of yellow are also present. As previously discussed, range detection threshold can be adjusted. Increasing this value will reduce the likelihood of false detection. However, the compromise is losing sensitivity to detect all possible objects in the field of view.

4.2 Range Capabilities

4.2.1 Return Intensity

Radar corner reflectors were used to characterise the maximum detectable range in ideal conditions. Parameters influencing range were fixed, only the radar cross section varies. The manufacturing error of each corner reflector was measured using a vernier protractor and vernier calipers. The percentage error of each corner reflector was measured for the 3 variables, a , $a\sqrt{2}$, and θ . Measured results are shown in table 4.1.

Table 4.1: Summary of corner reflector manufacturing error

Manufacturing tolerance of corner reflectors T1-4				
Target	RCS m^2	a (%) Error	$a\sqrt{2}$ (%) Error	θ (%) Error
T1	400	0.4	0.8	0.6
T2	200	0.3	0.7	2.0
T3	120	1.9	2.4	1.7
T4	60	0.4	0.4	2.0

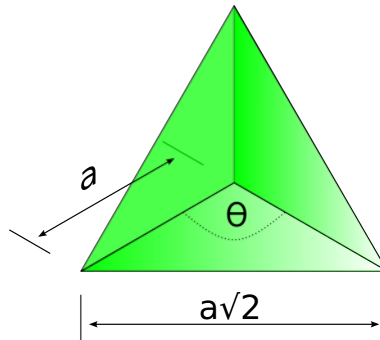


Figure 4.2: Triangular corner reflector

Parameters a and $a\sqrt{2}$ are critical for accurately determining radar cross section. In the context of these experiments, minor error in these parameters introduces minimal uncertainty when finding maximum range, provided the RCS is measured and determined. However, the physical nature of a corner reflector requires a 90 degree corner in order to bounce maximum power back towards the antenna. If θ error is too large, maximum power will not be directed towards the radar receiver, causing an inaccurate range measurement. Both, lengths and angle error are within acceptable limits, $\sim 2\%$ or less.

Experimental results showing maximum detectable range of 4 corner reflectors manufactured can be seen in figure 4.3. Results show range vs relative intensity to be a linear relationship. An attempt is made to explain the reason for this in subsection 4.5. The expected result is an decay following $1/R^4$. Following the RRE, *the received power is inversely proportional to R^4* . For example, if the range to the target is doubled, the received power is reduced to one sixth of the original. This of course is a measurement of the power at the receiver.

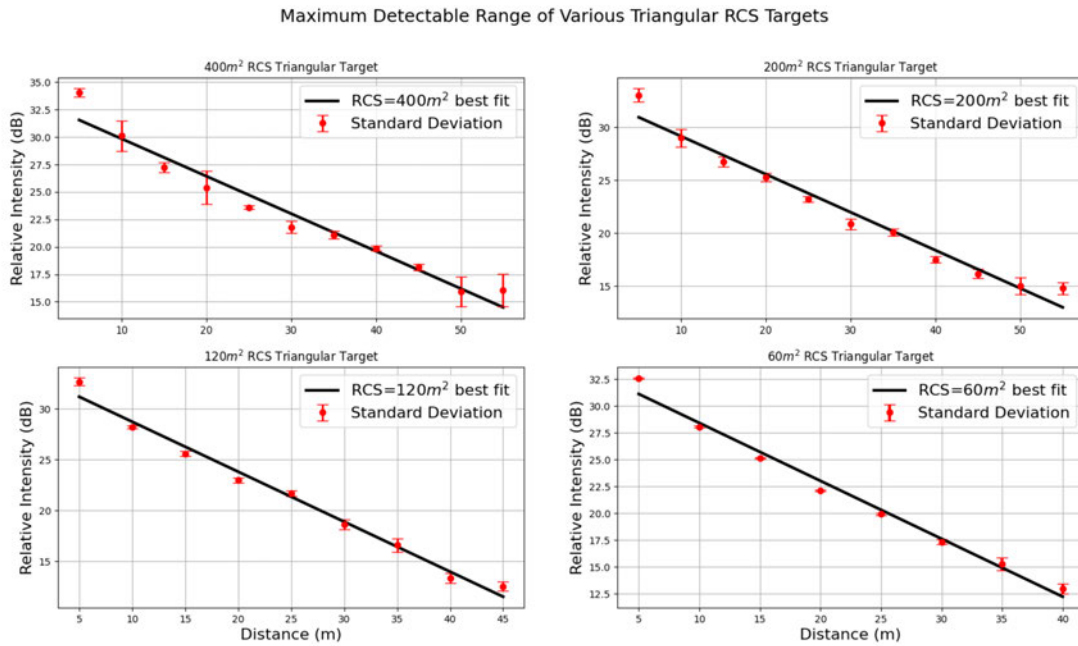


Figure 4.3: Maximum detectable range of fabricated corner reflectors

Results show the range detection threshold is approximately 15dB as expected from the configured chirp parameters. The significance of this parameter is later discussed in section 4.5. Maximum range of targets T1=400m² and T2=200m² both exceed the 50 meter maximum detectable range expected. Detectable range then drops to 45m and 40m for Targets T3=120m² and T4=60m² respectively. By this logic, each time the RCS is halved the detectable range will decrease by 5m (ie RCS=30 has a detectable range of 35m ect). However, to be certain this needs to be confirmed experimentally. The data capture time at each range was approximately 10-15 seconds which captures between 300-400 samples. The standard deviation of sampled data at each distance is displayed in red. It can be seen that error intensity is minimal throughout the full scale range. A maximum error of 0.6dB is present at and past full scale range of 50 meters for target T1. This is expected to occur as the radar approaches its range limitations. Interestingly

this same error is not present at the full scale range in target T2 results.

This can only be a result of two things. First, the radar target is not perfectly normal to the radar sensor when target T1 measurements were taken. Or, secondly, the 2° error in the parameter θ for target T2 had a positive influence on the result, decreasing the standard deviation in sampled data. The uncertainty of the former can be quantified in figure 4.6. The reduction in return signal due to an angular offset of 2 degrees is 0.3dB, an offset of 5 degree reduces return intensity by 0.6dB. This result goes some way in explaining the increase in error. Additionally, radar error will increase with range as the return signal is related to $\cos\theta$ of the reflector. This is depicted in figure 4.4, adjusting the angle reflector through θ off radar bore sight will decrease the relative return power received and recorded according to expression 4.1. The effect this has had on the results is difficult to quantify without without further experimentation.

$$P_r = P_t \cos(\theta) \quad (4.1)$$

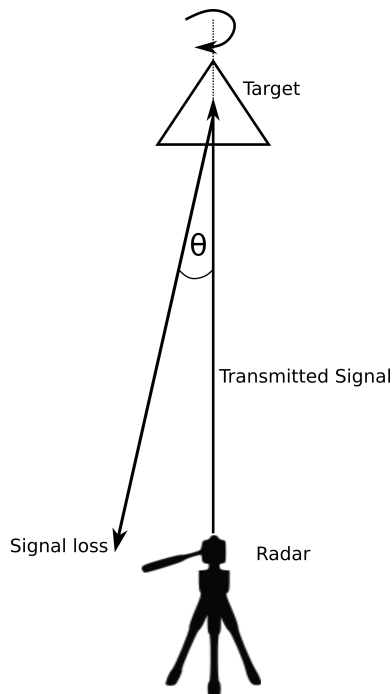


Figure 4.4: The signal loss due to angular misalignment increase with distance according to expression 4.1

4.2.2 Range Accuracy and Resolution

In addition to intensity, the radar can provide range information in cartesian coordinates. Range accuracy and resolution shown in figure 4.4 was evaluated from 5-55 meters inclusive. The standard deviation of sampled data in most locations is close to zero. At 40, 45 and 50 meters, standard deviation is exactly zero, therefore, the 0.8 meter error at 10 meters looks to be an anomaly. Radar range measurements (red y-axis) are compared against manual measurements (x-axis) taken at the same increments with a 75 meter tape measure. Radar range data deviating from the calibration line (shown in black), provides a measure of accuracy. The range error is in millimeters and is quantified in blue using the second y axis (blue y-axis). No distinguishable trend is shown in range error, this in large is caused by the experimental setup. The centre of the tripod is positioned approximately at the desired range when read off the tape measure. The error in this approximation could be 50mm, therefore making it hard to draw accurate conclusions on the source of the range uncertainty.

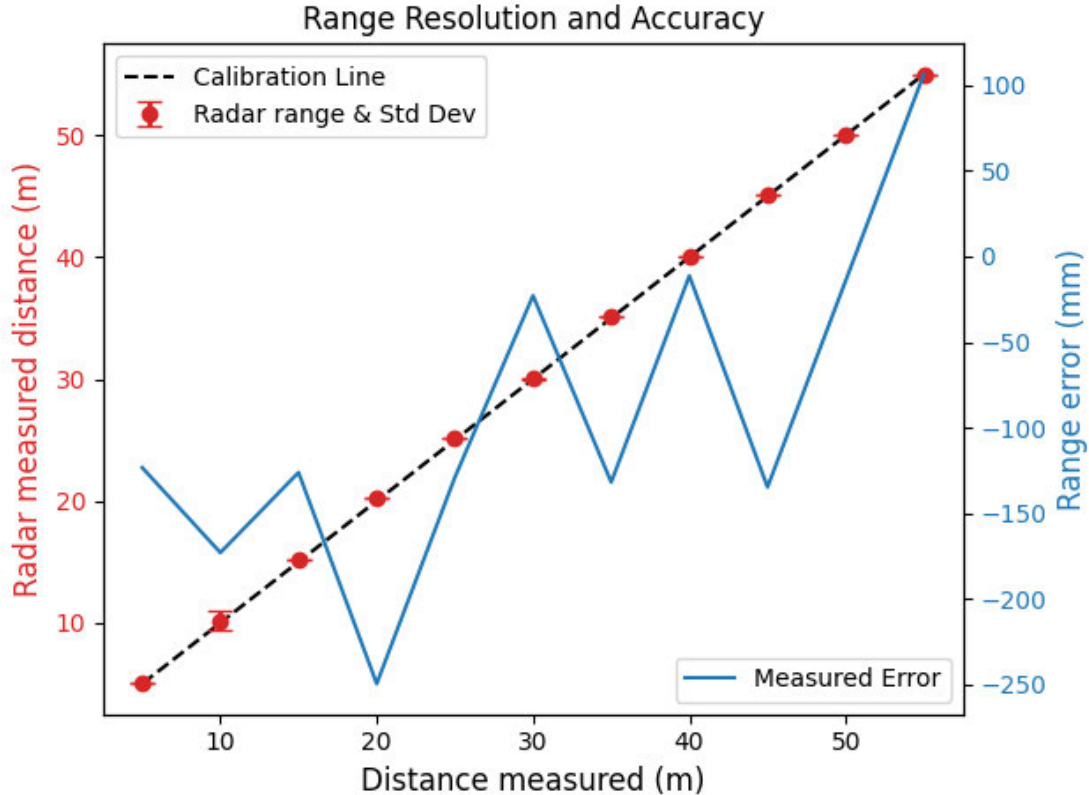


Figure 4.5: Range accuracy and resolution when measuring largest corner reflector, T1. Data includes uncertainty and the range error recorded by the radar at each location.

4.3 Peripheral Capabilities

Understanding peripheral capabilities in addition to range is vital in determining signal and sensor coverage around a vehicle. As outlined in subsection 3.5, a corner reflector was mounted and the radar was rotated through 0-180° in one degree increments. Results presented in figure 4.6 provide a comparison of the fitted experimental result and those published by Texas Instruments after digitising. Raw data collected shows a non symmetrical response between the captured range of $\pm 45^\circ$ off bore sight. A quadratic function is fitted, closely matching the fit produced by TI. A range of functions were trialled, the quadratic was selected as it most closely matches -3dB beam width published by Texas Instruments. The beam width of each configuration can be determined from these radiation patterns. Fitted experimental data at 76-77 GHz, based on a 3dB drop in intensity at a range of 15m as compared to bore sight, the horizontal -3dB beam width is approximately $+33.2^\circ$ and -29.8° . Comparatively, TI results at the same frequency but an unknown range with a 3dB drop in intensity compared to bore sight, the horizontal 3dB beam width is approximately $\pm 35.5^\circ$. TI's methodology for characterising the antenna in the horizontal plane, is not well documented. It can be assumed the experiment was conducted in an anechoic chamber, or at a minimum in a wide open space where minimal clutter or scatter is returned. Disregarding the signal offset, which is likely attributed to the environmental conditions, chirp parameters used and/or the range and size of the target, experimental data closely aligns. Therefore, the -3dB beam width can conservatively be approximated as 30° .

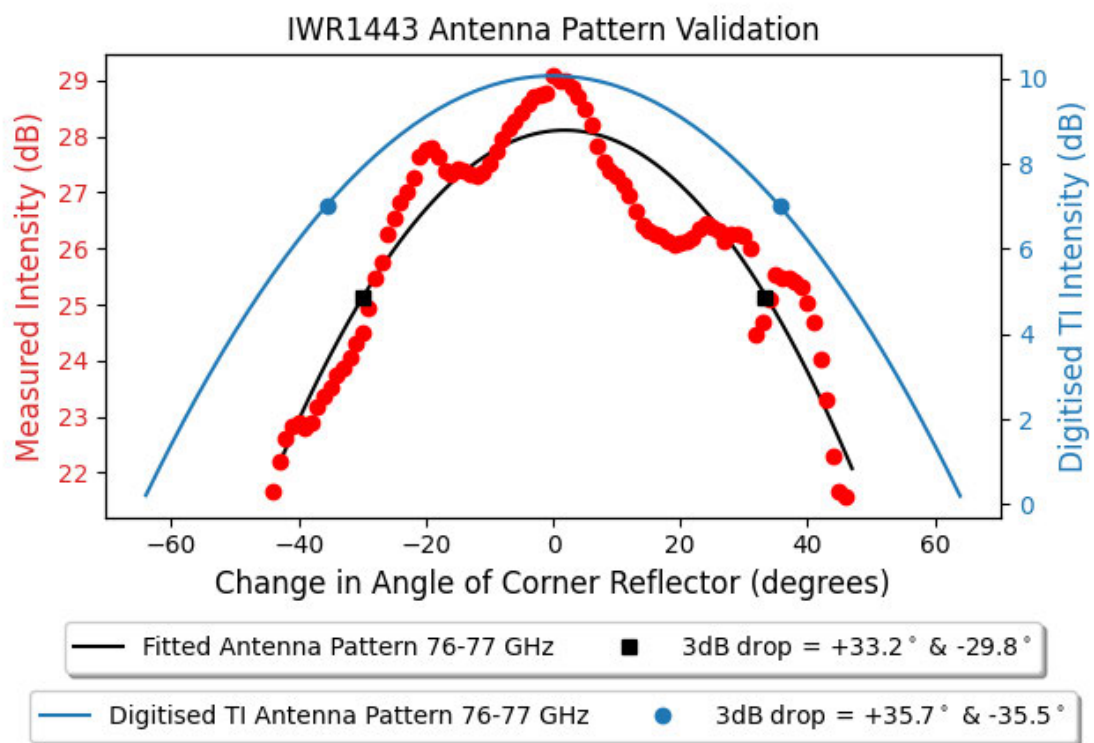


Figure 4.6: Experimentally measured and fitted horizontal antenna pattern against the same results published by Texas Instruments after digitising

4.4 Radar Cross Section Measurements

RCS is important for detecting and identifying hazardous objects in a fire environment. A key requirement for absolute situational awareness is understanding the objects range, bearing and elevation. Additionally, object identification and size are important for determining risk when performing situation assessments. Little literature exists in the space of detection and tracking of trees. Since falling trees are a common risk to fire fighting vehicles, RCS measurements have been recorded of both a standing and fallen tree. The experimental setup is shown in figure 4.7 and figure 4.9 with the corresponding data shown in figure 4.8 and figure 4.10 respectively.

The minimum detection threshold of 15dB was marginal for detecting and recording data, specifically for a fallen tree. Therefore, due to the material properties and uneven size/shape of the tree, return signal intensity was often significantly smaller than that received by a corner reflector.

For consistency across experiments, a 15 meter range was selected. Trees selected met the experimental requirement of reducing back scatter and clutter, meaning no major objects or reflective surfaces existed within the detectable range of 50m meters. To meet this requirement available trees could only be surveyed between 0 and 180 degrees. These experiments therefore assume the RCS is symmetrical about this axis. Physical size of each tree is represented in table 4.2. Trunk circumference and the radius of foliage from the trunk are measured manually with a tape measured, while height was estimated through photographs with an object of a known height in the frame for reference.

Table 4.2: Tree type and physical size of standing and fallen tree

Height and circumference of standing and fallen tree				
Orientation	Tree Type	Trunk Circumference	Height	Radius foliage extends from the trunk
Standing	Eucalyptus	3.9m	13m	5m
	melliodora			
Fallen	Eucalyptus	2.5m	12m	5m
	melliodora			



Figure 4.7: Standing tree selected for RCS and range measurements. The orientation of the tree relative to the result is also shown.

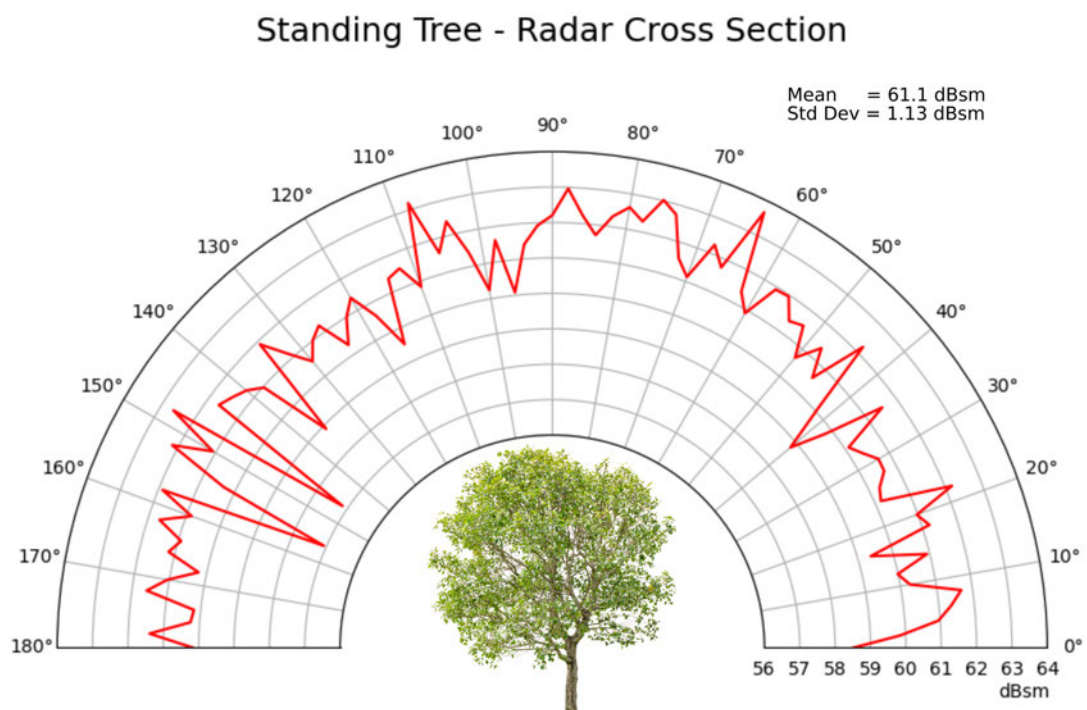


Figure 4.8: Radar Cross Section measurement of standing tree in dBsm

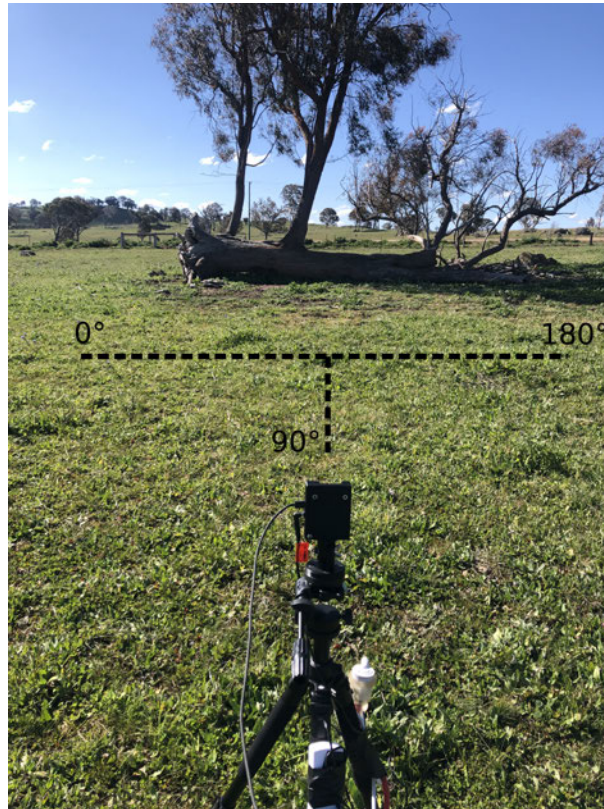


Figure 4.9: Fallen tree selected for RCS measurements. The orientation of the tree relative to the result is also shown.

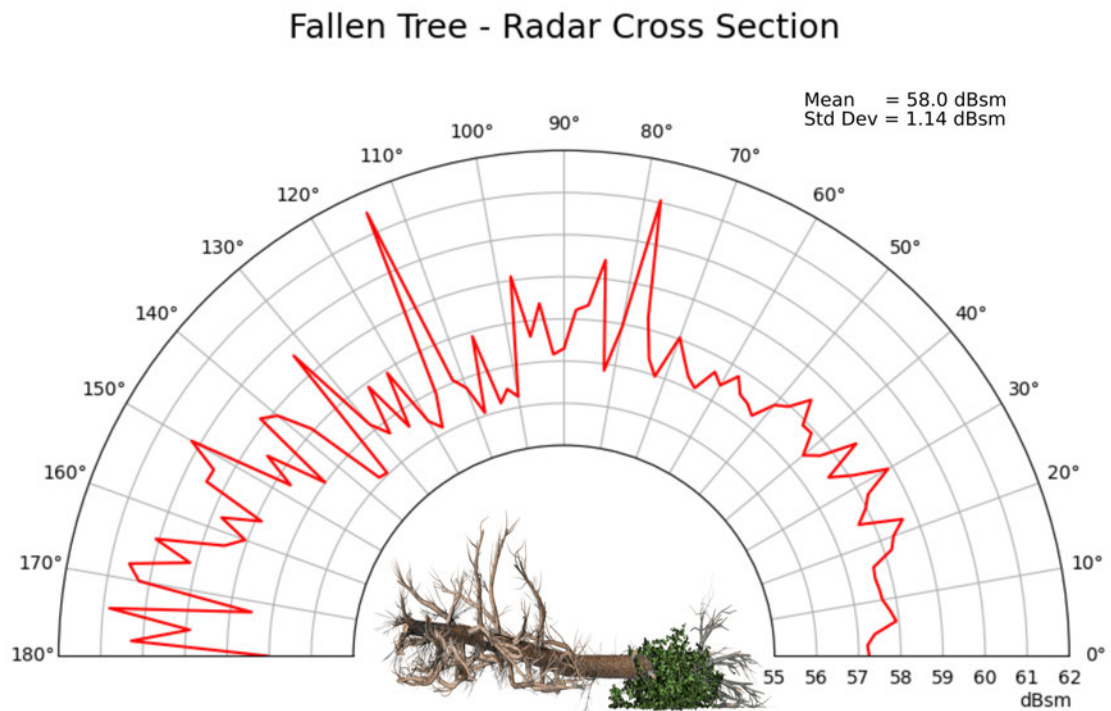


Figure 4.10: Radar cross section measurement of fallen tree in dBsm

RCS of a standing tree with the measurements shown in table 4.2 is depicted in figure 4.8. Mean RCS is evaluated as 61.1 (relative) dBsm with a standard deviation of 1.13 (relative) dBsm. As the radar antenna only has a 15 degree elevation capability, it is possible little foliage reflections are recorded. Therefore, reflections recorded are mostly due to inconsistencies in shape and texture of the trunk and branches. Between the angles of 0 and 60 degrees where low hanging branches and foliage are noticeable, *possibly* results in a more consistent RCS. Where the trunk is more exposed at angles greater than 130, RCS is more variable. Uncertainty around this hypothesis could be reduced with further experiments to understand measurement repeatability.

The RCS of the fallen tree depicted in figure 4.10 shows the roots are oriented perpendicular to the radar at zero degrees. Mean RCS is 58.0 (relative) dBsm with a standard deviation of 1.14 (relative) dBsm. Reflections from zero to 75 degrees were weak, causing a lower RCS. This could be attributed to the highly jagged and irregular shape the trees root structure. Reflections from 75 to 180 degrees are elevated and highly inconsistent. As foliage of the fallen tree is closer to the ground, (within 15 degrees of elevation) signals have reflected and been detected by the radar. This is likely the cause of the increased RCS from 75 to 180 degrees.

Analysing the RCS polar diagrams for both a standing and fallen tree, it is not possible to conclusively differentiate between the two based only on the RCS data. With mean and standard deviation so closely matched and major inconsistencies throughout both diagrams, more reliable information is required in order to accurately identify the difference.

4.5 Object Identification & Range Prediction

Results presented in subsection 4.2 show the influence of RCS on detectable range. This can be further elaborated to predicted the type of object detected. Fitted maximum detectable range vs relative power of the 4 corner reflectors is shown in figure 4.11. Additionally, range data recorded of the standing tree is also presented.

4.5.1 Detecting Range of Standing Tree

Comparatively, standard deviation of sampled data of a standing tree is much higher than that recorded of each corner reflector. The greatest (1.9 relative dB) is found to be at the closest range of 5 meters. At the largest recorded range of 45 meters the standard deviation is 0.68 (relative)dB. This is characteristic of a trees shape and material. The vector diagram depicted in figure 4.12 (a) and (b) provides an elementary explanation of the counter intuitive reduction in standard deviation as range increases.

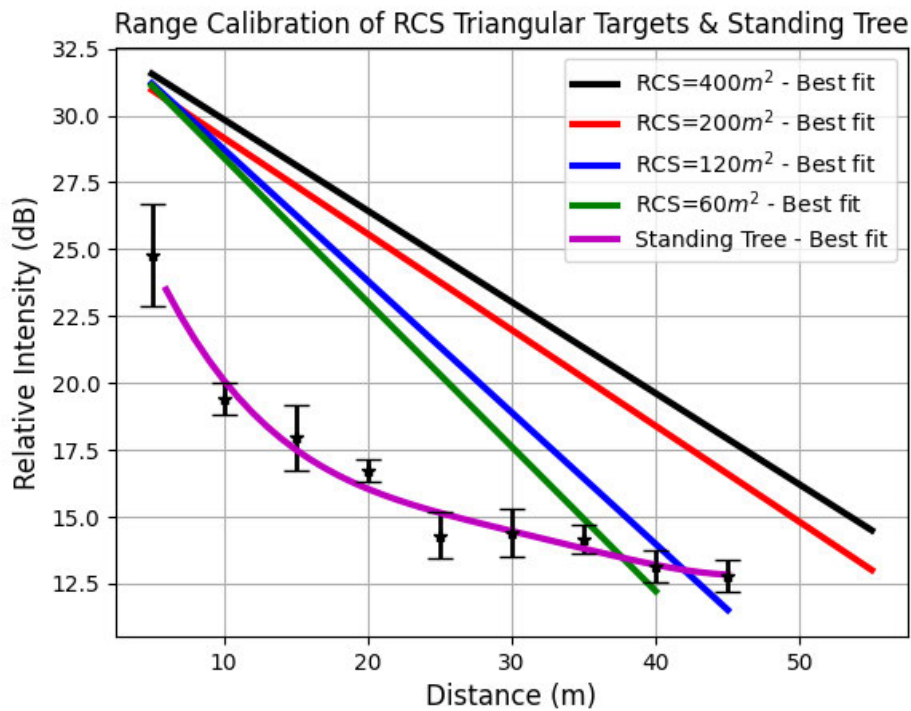
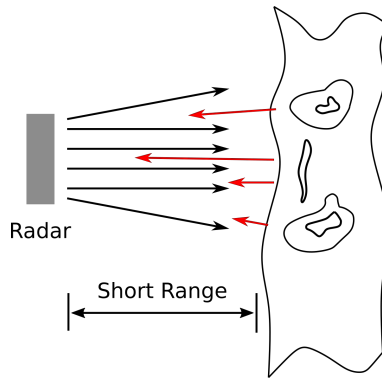
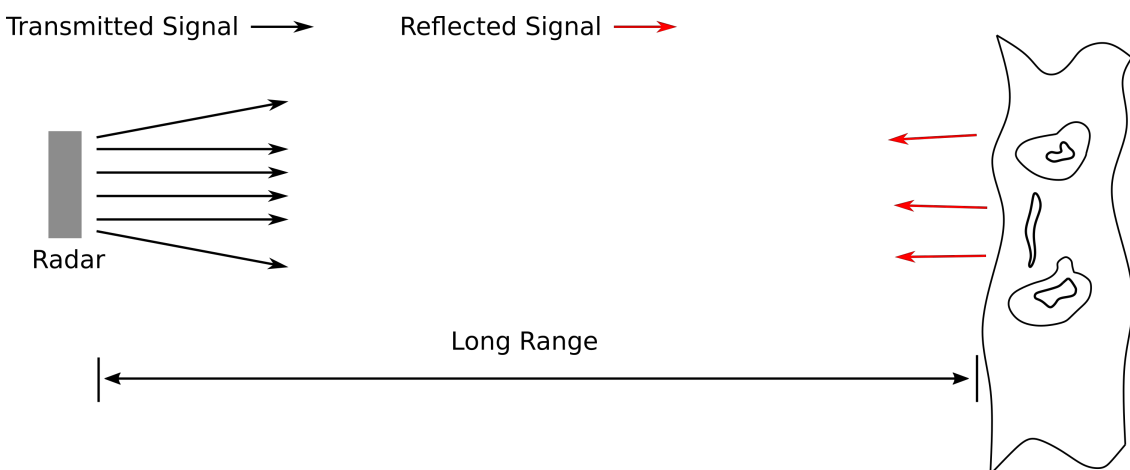


Figure 4.11: Range measurement best fit of known RCS's

With a beam width of 30 degrees, at short range, signals are reflected from scrolls knots and shape inconsistencies in the trees trunk back toward the receiver. Each reflection will have some kind of loss due to the nature of the reflective surface. Variation in this loss and change in angle of the reflection is one plausible reason for the high standard deviation. At long range, the tree trunk acts similar to a corner reflector, mostly detecting normal signals. This is further supported when analysing the length of data sets at each distance over approximately the same time duration. Over 10 seconds, at 5 meters a total 158 samples are recorded, at 45 meters a total of 4 samples are recorded. Following the expression for standard deviation, this large discrepancy in data length would also be a large contributor to the difference in uncertainty. To be certain of the percentage contribution from each possibility, more data is required.



(a) Vector diagram showing short range reflections from a tree trunk



(b) Vector diagram showing long range reflections from a tree trunk

Figure 4.12: Radar data visualised

4.5.2 Object Identification

Point cloud data presented in figure 4.1 shows reflection intensity at a known range can be identified and used to improve object identification algorithms. Results shown in figure 4.11 demonstrates this is feasible at ranges greater than 20-30 meters. At a range of 5 meters, maximum return intensity is received by all 4 corner reflectors. As range increases the returning intensity starts to differ. The experiment assumes environmental conditions and sensor error remains constant across all data sets. Therefore, change in slope of each curve can only be attributed to the change in radar cross section. Noticeably, the reported RCS of a standing tree (61dBsm) in subsection 4.4 does not align with the recorded results of the $60m^2$ corner reflector. This is attributed to RCS measurements of standing and fallen tree experiment reported in relative dBsm. This result demonstrates, at a range greater than approximately 20 meters relative intensity is valuable information in helping to identify objects.

4.5.3 Range Prediction using RRE

Evaluating range capability and accuracy of a known chirp parameter is useful. However, a distinct advantage of the IWR1443 sensor is chirp parameters are programmable. Therefore, if fire conditions were to change, chirp parameters could be optimised to suit the current conditions or situation. To determine the efficacy of predicting range with IWR1443 platform, the experimental results were compared with predictions based on the radar range equation 4.2.

$$P_{r(\text{theoretical})} = \frac{P_t G_t G_r \lambda^2 \sigma}{(4\pi)^3 R^4} \quad (4.2)$$

The validation makes a number of assumptions, the radar range equation assumes one hundred percent of the energy transmitted is intercepted by the target and reflected back toward the antenna. Additionally, power return is assumed to be read from the receiver, not accounting for minimum detectable power, signal to noise ratio (SNR), receiver bandwidth, temperature variation or receiver noise. However, data produced by the Texas Instruments radar platform does account for these parameters, meaning this result will not be perfectly comparable. Intensity data recorded with the IWR1443 is relative to the

minimum detectable power at the receiver, described by the expression:

$$P_{RX,min} = kTB_rF(SNR)_{min} \quad (4.3)$$

The parameter values required for the analysis were obtained from TI's IWR1443 data (Texas Instruments n.d.) sheet shown in table 4.3.

Table 4.3: Radar parameters for experimental validation.

Height and circumference of standing and fallen tree			
Parameter	Value	Parameter	Value
P_t	12 dBm	k	1.38×10^{-23}
G_t	1	T	290° K
G_r	24 dB	B_r	15 MHz
λ	0.0038961 m	F	15dB
σ	$61m^2$ & $400 m^2$	$(SNR)_{min}$	2dB

Utilising equation 4.3, the calculated $P_{RX,min} \approx 1.50789 \times 10^{-12}$ W. To accurately compare the theoretical and experimental results, theoretical units were converted to relative intensity using expression 4.4.

$$P_{r(Relative)} = \frac{P_r(theoretical)}{P_{RX,min}} \quad (4.4)$$

Data validation using the above equations is presented in figure 4.13. Two experimental results are compared against 2 theoretical calculations. The radar cross sections selected were T1 ($400m^2$) and the experimentally found standing tree (61 dBsm). As expected, the theoretical result decays with distance following the $1/R^4$ rule. The experimental data however follows an almost linear path as distance increases, showing the experimental data is incompatible with the theoretical calculation. The reason for this is still not known but could be attributed to a number of things, including:

1. Assumptions made in the theoretical calculation do not account for experimental effects.
2. Theoretical parameters are not accurately represented. Traditionally transmit power would be actively monitored and recorded throughout the experiment. For this validation we have chosen a mean P_t value of 12 dB as specified by data sheet. Additionally, it is possible the radar has automatic gain control.
3. It is not fully understood, the TI platform possibly has an optimisation algorithm that linearises data to make for more accurate range estimation.
4. It is possible the signal is saturated. However, this can some what be ruled out using the results presented in appendix A.

After applying an 4th order fit, it is obvious the simplest form of the RRE is not a suitable method of determining range parameters for the TI platform. Before a theoretical design approach can be applied, a more in depth analysis is required. Until then, to design a system to meet conditions outside of the norm, an empirical approach is required.

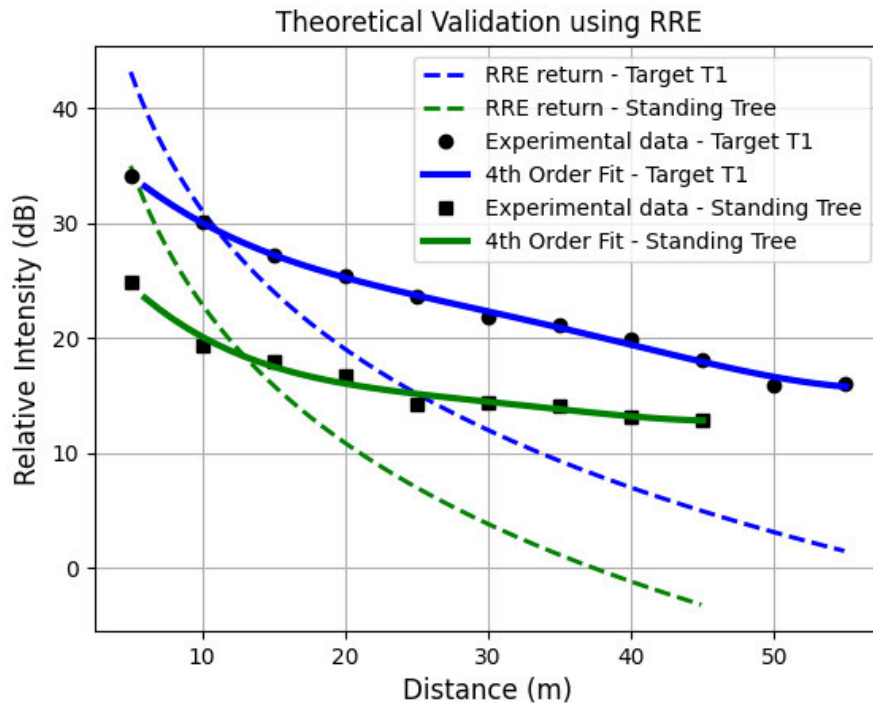


Figure 4.13: Theoretical and experimental range comparison using the Radar Range Equation. In this instance, a 4th order fit was used to demonstrate the linearisation after 25 meters.

4.6 Discrete Discussion

The novel idea of this research is using newly available automotive mm-wave radar technology on fire fighting vehicles. Previous research investigated mm-wave radar technology in a fire environment for use in robotics. For urban fire environments; (Starr & Lattimer 2014) show its feasibility. In the work presented, we have demonstrated ROS's use as a platform to integrate this sensor into robotics or future sensor system applications. This research applies to other industries, including; the agriculture, medical and transport industries.

The results show the accuracy and reliability of the radar. Quantifying the repeatability of results compared to those published by the manufacturer is fundamental to informing future sensor system design. Using the maximum detectable range and horizontal antenna pattern results presented, designers can estimate the detectable range of a known RCS at any specified angle within the field of view. This information can be used as a guide for a new sensor system design. For example, an RCS of 60m^2 must be detectable at a minimum of 25 meters and 30 degrees. Therefore, using the data above, a 60m^2 RCS has a return intensity of 22.5 dB at 25 meters when on radar bore sight. At an angle of 30 degree off bore sight the relative intensity will drop by -3dB. Therefore the expected return intensity in this scenario will be 19.5 dB.

Further, the evaluation of radar cross-section of organic objects found in a fire environment is a new contribution to the field. Specifically, native trees pose the biggest threat to firefighter safety. (Mougin et al. 1993) showed that RCS scatter was different at the base of a tree architecture compared to the leafy foliage higher up. The advancement this work made to the field was the influence of a trees orientation to the radar. When visibility is low, it is important to be able to predict the risk an object poses. Results show a different RCS pattern for the two orientations; however, the mean and standard deviation hover around the same value. This demonstrates the RCS is too similar for mm-wave radar to differentiate between the two orientations without some additional sensing capability such as IR machine vision. To further understand the influence of orientation, more experiments at various distances from the tree are required. Such experiments expose more of the vertical tree's foliage, potentially providing a different, more meaningful result.

Chapter 5

Conclusions & Future Work

5.1 Introduction

This project has performed fundamental experiments for the design and development of a radar system for fire fighting vehicles. The primary purpose of the experiments was to determine the maximum and minimum capabilities of the Texas Instruments IWR1443 radar platform with controlled parameters and ideal conditions. These results were then contextualised for fire fighting by extending the experimental campaign into testing objects unique to a fire environment. The results of both the controlled and fire specific experiments were then validated against the commonly used radar range equation. This chapter summarises the outcomes and conclusions and discusses recommendations for future work.

5.2 Maximum Detectable Range and Peripheral Capabilities

The first objective of work undertaken was to determine the most appropriate sensing technology for a fire environment and perform basic testing to understand its capabilities. As discussed in chapter 2 mm-wave sensing is now an affordable and promising technology with high resolution and accuracy. The technology is insensitive to environmental conditions such as smoke, fog, dust, and luminosity. Results presented in section 4.1

shows sensor information can be accurately presented in a spatially resolved environment to show hazards and objects in the path of the instrument's radiation.

In line with research objective number 2, '*determine the maximum detectable range and accuracy of selected sensing technology.*' Relevant chirp parameters were selected, and the maximum detectable range and range accuracy was evaluated under controlled conditions with known radar cross sections. Results show the maximum detectable range exceeds that specified by the Texas Instruments online chirp parameter calculators for RCS's larger than $200m^2$. Additionally, the range accuracy is highly reliable, with millimetre accuracy at the maximum range of fifty meters.

For situational awareness, it is important the peripheral capabilities are understood. Experimental results presented in 4.3 shows the maximum/minimum angle objects can be detected in the 76-77GHz frequency band is approximately 30 degrees. This result informs the position and number of radar sensors required around a fire fighting vehicle to achieve maximum information in order to increase situational awareness. Additionally, the combination of range and peripheral data provides a guide for the expected return intensity for a known RCS at a specified angle within the field of view.

5.3 Radar Cross Section Measurements

An important capability in a fire environment is the detection and tracking of trees and potentially hazardous objects. For a radar sensor, this requires an in-depth understanding of said object's radar cross section. Radar cross section measurements taken of standing and fallen trees presented in chapter 4.4, show the return intensity at orientations zero to one hundred and eighty degrees. Using standard deviation and mean calculations, it has been determined that RCS of a standing and fallen tree are similar. Proving return intensity data cannot adequately resolve the orientation of a tree. However, it does show a tree's RCS is significantly different from that of a vehicle or metal-based object, proving the two objects could be identified in a real-life scenario.

In order to validate the detectable range of known radar cross-sections, experimental results were compared against simulated results calculated with the same parameters using the radar range equation. Results presented in subsection 4.5 show the simulated results follows the expected trend of $1/R^4$. Experimental results however, are mostly

linear. This shows that the traditional design approach using the radar range equation will not produce reliably accurate results. Therefore an empirical approach is required when further designing a radar system for fire fighting vehicles.

5.4 Future Work

To further advance this technology, future fundamental experimentation needs to be undertaken to evaluate the effect of different chirp parameters. This includes varying the transmit power and the receiver gain to see the effect on accuracy and detectability. Following this, work can be performed that investigates the effect of performing similar test under dynamic conditions, ie mounted onto a vehicle. This will show the influence of vibration and a how detection varies when the radar is continuously moving. This can then be followed by research into sensor fusion of the radar with other promising technologies. One promising combination is the fusion of radar with GPS, this opens the possibility to extend the solution of situational awareness to a global crew wide level, across multiple vehicles. The ability for trucks to detect a risk and then communicate this to other vehicles in the fleet would be invaluable. Other work worth investigating is the fusion of multiple mm-wave radar sensors, this would allow multiple sensors to be mounted around the vehicle, providing 360° spatial information.

References

- Altman, B. (2012), 'Understand fire behavior to improve your situational awareness', *Fire Engineering* **165**(10), 79–80.
URL: <http://search.proquest.com/docview/1113775727/>
- Amon, F., Hamins, A., Bryner, N. & Rowe, J. (2008), 'Meaningful performance evaluation conditions for fire service thermal imaging cameras', *Fire Safety Journal* **43**(8), 541–550.
- Baum, T., Thompson, L. & Ghorbani, K. (2011), Measurement of radar cross-section and complex dielectric properties of forest fire ash, in '2011 8th European Radar Conference', pp. 349–352.
- Bel Kamel, E., Peden, A. & Pajusco, P. (2017), Rcs modeling and measurements for automotive radar applications in the w band, in '2017 11th European Conference on Antennas and Propagation (EUCAP)', pp. 2445–2449.
- Bradstock, R. A. (n.d.), *Flammable Australia : fire regimes, biodiversity and ecosystems in a changing world*, CSIRO Pub., Collingwood, Vic.
- Buddendick, H. & Eibert, T. F. (2010), 'Acceleration of ray-based radar cross section predictions using monostatic-bistatic equivalence', *IEEE Transactions on Antennas and Propagation* **58**, 531–539.
- Bush Fire Danger Period and Fire Permits* (n.d.).
URL: <https://www.rfs.nsw.gov.au/fire-information/BFDP>
- Clark, S. & Dissanayake, G. (1999), 'Simultaneous localisation and map building using millimetre wave radar to extract natural features', *Proceedings - IEEE International Conference on Robotics and Automation* **2**, 1316–1321.

- Constapel, M., Cimdins, M., Hellbrück, H. & Lübeck (2019), ‘Practical toolbox for getting started with mmwave fmcw radar sensors’, *Proceedings of the 4th KuVS/GI Expert Talk on Localization*.
- CopRadar (2018), ‘Vehicle reflection’, <https://copradar.com/chapts/chapt3/ch3d6.html>. [Online; accessed July-2020].
- Faulconbridge, R. I. (2002), ‘Radar fundamentals’.
- Großwindhager, B (2019), ‘The potential of low-cost millimeter-wavesensors for mobile radar applications’, https://static1.squarespace.com/static/559921a3e4b02c1d7480f8f4/t/5d4a91c2e6cf6c000129fbb8/1565168078616/Grosswindhager+Bernhard_+868.pdf.
- Gubana, B. & Southern, A. G. (2017), ‘Coroner finds no one factor to blame for wa firefighter death’.
URL: <https://www.abc.net.au/news/2017-06-22/coroner-finds-no-one-factor-death-firefighter-wendy-bearfoot/8643652>
- IWR1443BOOST Evaluation Module mm-Wave Sensing Solution* (2018).
URL: <http://www.ti.com/lit/ug/swru518c/swru518c.pdf?ts=1590298418429>
- Jolly, W. M., Cochrane, M. A., Freeborn, P. H., Holden, Z. A., Brown, T. J., Williamson, G. J. & Bowman, D. M. J. S. (2015), ‘Climate-induced variations in global wildfire danger from 1979 to 2013’, *Nature Communications* **6**(1), 7537.
- Kim, J.-H., Starr, J. & Lattimer, B. (2015), ‘Firefighting robot stereo infrared vision and radar sensor fusion for imaging through smoke’, *Fire Technology* **51**(4), 823–845.
- Kim, T., Kim, S., Lee, E. & Park, M. (2017), Comparative analysis of radar-ir sensor fusion methods for object detection, in ‘2017 17th International Conference on Control, Automation and Systems (ICCAS)’, Vol. 2017-, Institute of Control, Robotics and Systems - ICROS, pp. 1576–1580.
- Klein, G. A., Calderwood, R. & Clinton-Cirocco, A. (1986), ‘Rapid decision making on the fire ground’, *Proceedings of the Human Factors and Ergonomics Society Annual Meeting* **30**(6), 576–580.
- Longbottom, J. (2015), ‘system failed’ two firefighters killed by falling tree: coroner’.
URL: <https://www.abc.net.au/news/2015-12-17/system-failed-two-firefighters-killed-by-falling-tree-coroner/7038868>

- Maxwell, F. (1971), 'A portable ir system for observing fire thru smoke', *Fire Technology* **7**(4), 321–331.
- Mougin, E., Lopes, A., Karam, M. & Fung, A. (1993), 'Effect of tree structure on x-band microwave signature of conifers', *IEEE Transactions on Geoscience and Remote Sensing* **31**(3), 655–667.
- Mrdakovic, B. L., Olcan, D. I. & Kolundzija, B. M. (2015), Full-wave modeling of stochastic trees for radar cross section calculation, *in* '2015 9th European Conference on Antennas and Propagation (EuCAP)', pp. 1–4.
- 'Much-loved' firefighter and father of two killed working on Victorian blaze (2020).
URL: <https://www.abc.net.au/news/2020-01-11/victorian-firefighter-dies-in-omeo/11860722>
- of Meteorology, B. (n.d.), 'Climate change trends and extremes'.
URL: <http://www.bom.gov.au/climate/change/>
- Omine, Y., Sakai, M., Aoki, Y. & Takagi, M. (2004), Basic examination of a technique to visualize space filled with dense smoke using millimeter wave radar, Vol. 5603, pp. 272–281.
- Press, A. A. (2019), 'Nsw bushfires: Rfs names two firefighters killed south-west of sydney'.
URL: <https://www.theguardian.com/australia-news/2019/dec/20/nsw-bushfires-rfs-two-firefighters-killed-south-west-sydney>
- Radiation Protection Standard* (2002).
URL: <https://www.arpansa.gov.au/sites/default/files/legacy/pubs/rps/rps3>
- Rao, S (2017), 'Introduction to mmwave sensing: Fmcw radars', <https://training.ti.com/intro-mmwave-sensing-fmcw-radars-module-1-range-estimation>.
- Second firefighter dies within weeks in SA* (2017).
URL: <https://www.abc.net.au/news/2014-12-10/second-firefighter-death-in-sa-investigated-rendelsham/5956288>
- Speal, N. (2013), 'Converting ros bag to csv', <https://www.clearpathrobotics.com/assets/guides/kinetic/ros/Converting%20ROS%20bag%20to%20CSV.html>. [Online; accessed Aug-2020].

Starr, J. & Lattimer, B. (2014), 'Evaluation of navigation sensors in fire smoke environments', *Fire Technology* **50**(6), 1459–1481.

Texas Instruments (2018), 'Mmwave sdk user guide', <https://www.ti.com/tool/MMWAVE-SDK>.

Texas Instruments (n.d.).

Tutorial, R. (2020), 'Radar cross section', <https://www.radartutorial.eu/01.basics/Radar%20Cross%20Section.en.html>. [Online; accessed July-2020].

Zhang, L. (2019), 'Ti mmwave ros package (customized)'.

Chapter 6

Project Specification

ENG 4111/2 Research Project

Project Specification

For: **Matthew Barrett**

Topic: Implementation of mm-Wave Radar for Increased Situational Awareness and Obstacle Avoidance on Fire Trucks

Supervisor: Craig Lobsey

Sponsorship: Faculty of Health, Engineering & Sciences, USQ

Major: Mechatronic Engineering

Enrolment: External (Online) S1-S2 2020

Project Aim: The overall aim of the project is to evaluate if millimetre wave sensing technology can improve the situational awareness of firefighters when driving through dangerous conditions. This will involve implementing a portable millimetre wave (mm-wave) sensing module along with a LCD display onto an emergency vehicles. Testing will be conducted in various conditions and in a variety of scenarios in order to determine the effectiveness of the technology for this application.

Program:

1. Perform back ground research on the current state of the art in this space.
2. Critically examine how the current state of the art is used and the potential gaps mm-wave sensing could fill.
3. Perform basic testing to understand the limitations of the mm-wave radar module.
4. Design portable hardware that will mount inside the vehicle. In addition, write the software that will process the incoming signal from the sensor and display this data to a graphical user interface (GUI).

5. Test the feasibility of the system by implementing it onto a vehicle to perform testing in various conditions. The testing will involve:
 - (a) Testing the effect vibration has on detection reliability by driving in 'off-road conditions'.
 - (b) Testing the maximum detectable range of a variety of objects, including; humans other vehicles and trees. Testing will be performed in both standard safe conditions and in hazardous smoke conditions while mounted to a moving vehicle.

As time and resources permit:

1. Perform situational awareness tests by placing a number of different drivers into a challenging scenario without regular driving aids and only the radar to guide them.
2. Perform basic testing in a heated environment to understand the variation in return signal when used in high temperatures.
3. Investigate implementing long wave infrared cameras in addition to mm-wave radar to further improve situational awareness.

Agreed:

Student Name: Matthew Barrett

Date: 15/03/20

Supervisor Name: Dr Craig Lobsey

Date:

Chapter 7

Radiation Safety Assessment

7.1 Risk Management Calculations

A thorough check of non-ionising radiation levels output by the radar system has been investigated to ensure it falls within safe exposure limits and regulations. According to the IWR1443 users guide, the module is in compliance with the European Safety Standard 2014/53/EU. The compliance has been verified in the operating bands 76-77GHz and 77-81GHz (*IWR1443BOOST Evaluation Module mm-Wave Sensing Solution* 2018). According to the European standard the user is safe provided a minimum distance of 5cm from the antenna is respected. Using the testing conditions for obtaining European certification, calculations were performed to ensure this module complies with the Australian Radiation Protection Standard for Radio Frequency Fields 3kHz to 300 GHz. The onboard antenna has a peak gain of 10.9 dBi. The typical testing conditions used to gain certification in Europe are as follows:

- 76-77 GHz band (2 antennas at a time) at the maximum peak power of $26dBm$
- 77-81 GHz band (1 antenna at a time) at the maximum peak power of $21dBm$

Converting the output power figures specified into Watts we have:

$$P_{W_{1Tx}} = \frac{1 * 10^{\left(\frac{26+10.5}{10}\right)}}{1000} = 4.4668W$$

$$P_{W_{2Tx}} = \frac{1 * 10^{\left(\frac{21+10.5}{10}\right)}}{1000} = 1.4125W$$

In the experiments outlined there is no possible way a person should be within a distance of 0.5m of the radar. Therefore, calculating the power density on the target at 0.5m and using the maximum output power levels specified above:

$$P_{density_{1Tx}} = \frac{0.9617}{4\pi(0.5)^2} = 0.8771W/m^2$$

$$P_{density_{2Tx}} = \frac{0.1259}{4\pi(0.5)^2} = 0.27741W/m^2$$

These calculated levels are more than 10,000 time less than that specified in the Australian Radiation Protection and Nuclear Safety Safe Exposure Limits Standard (*Radiation Protection Standard* 2002). The safe exposure limits outlined in this document can be seen in table 7.1.

Table 7.1: Basic restrictions for time averaged and instantaneous incident power flux density
(*Radiation Protection Standard 2002*)

Australian power flux density limitations			
Exposure Category	Frequency Range	Time Averaged Power Flux Density W/m ²	Instantaneous Power Flux Density W/m ²
Occupational	6GHz - 300GHz	50	50,000
General Public	6GHz - 300GHz	10	10,000

Chapter 8

Results utilising Mid-Range Chirp Parameters

8.1 Introduction

Prior to completing the results presented, experiments were undertaken using mid range chirp parameters. The mid range chirp parameter prioritised velocity resolution, experiments were conducted using the same corner reflectors presented in chapter 3.

8.2 Mid-Range Chirp Parameters

Table 8.1: Summary of chirp parameters, and resulting radar accuracy and resolution

IWR1443 Chirp configuration - 50m range	
Front end Configuration	
Idle Time	33.33 μ s
Frequency Start	76 GHz
Tx Start Time	1 μ s
ADC Valid Start Time	3.8 μ s
ADC Sampling Time	0
Frequency Slope	5.25 MHz/ μ s
Ramp End Time	61.8 μ s
Resulting parameters	
Number Tx	2 Antennas
Rx Gain	30 dB
Range Resolution	0.18m
Max Doppler Velocity	7.935 m/s
Max Allowed Elevation	90deg
Max Allowed Azimuth	90deg
Max Range	37.454m

8.3 Results

As shown in figure 8.1, the standard deviation and the returning trend is similar to that utilising long range parameters. The key finding in the results presented in chapter 4 is the unexpected linear relationship of intensity vs range. The results presented below demonstrates that this relationship is not a result of the chirp parameters. Furthermore, a similar linear relationship of intensity vs range of a standard utility vehicle presented in figure 8.2, showing the cause is not due to corner reflector properties or design. Therefore, from this result we can infer the relationship cannot be a case of signal saturation. Further experiments undertaken using the midrange chirp parameter with small corner reflectors also showed this linear relationship, removing the possibility that signal is saturated from large objects.

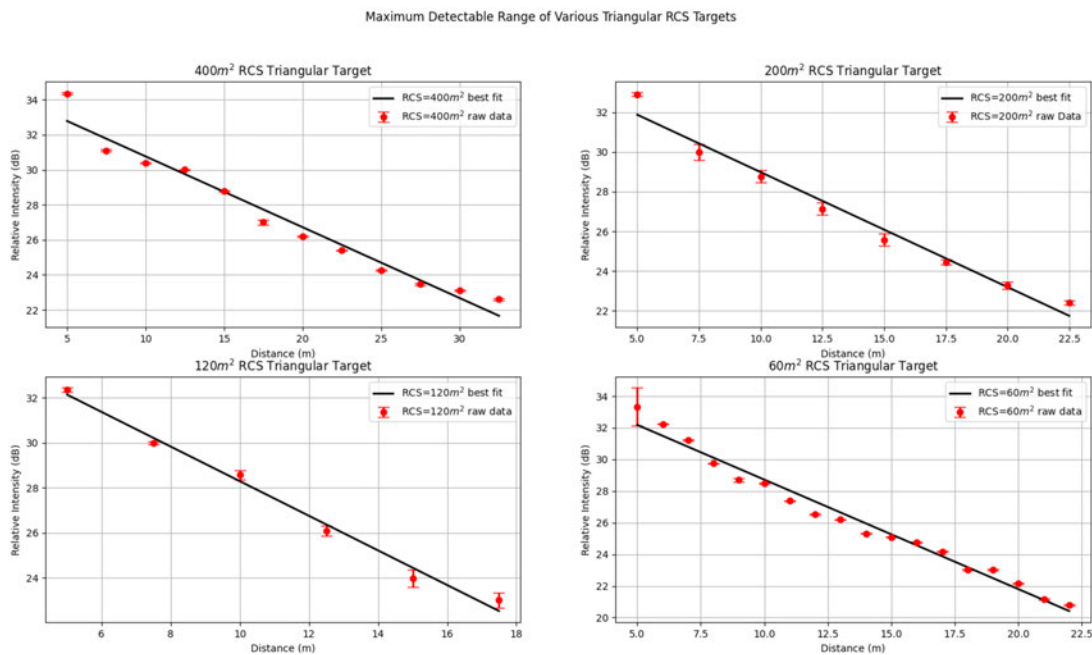


Figure 8.1: Maximum detectable range of the corner reflectors using mid range chirp parameters

An interesting finding in these results is the poor range accuracy. This is expected with a chirp parameter that is focussed on velocity resolution, however the inaccuracy is much larger than expected, as shown in figure 8.4.

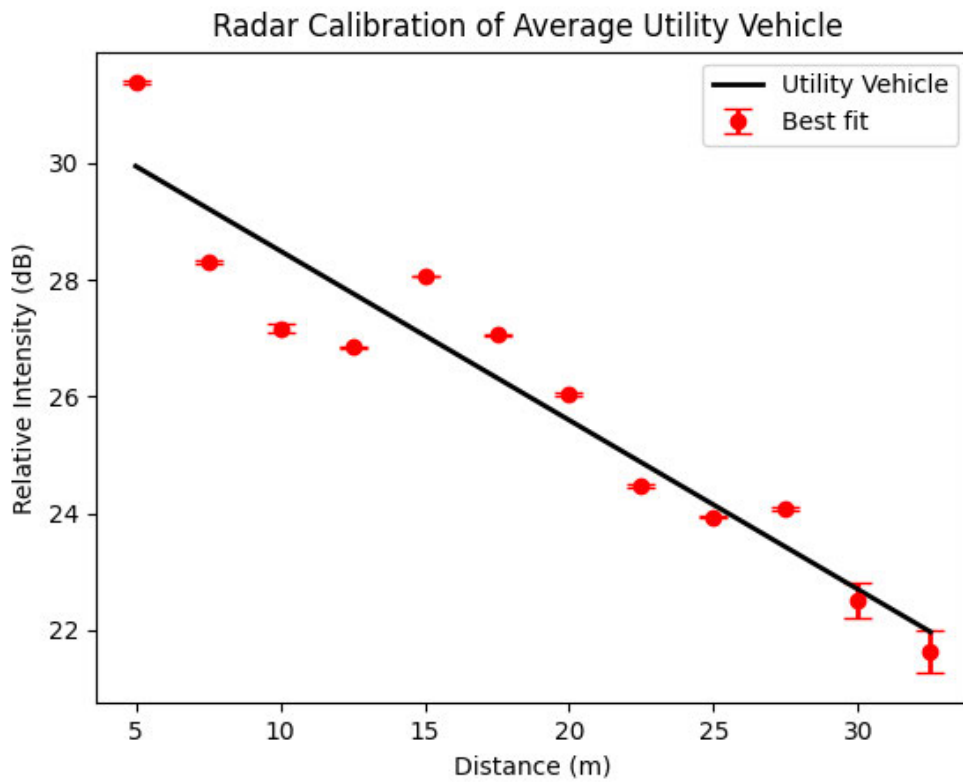


Figure 8.2: Experimental result of maximum detectable range of a utility vehicle using mid-range chirp parameters



Figure 8.3: Experiment evaluating the maximum detectable range of a utility using mid-range chirp parameters.

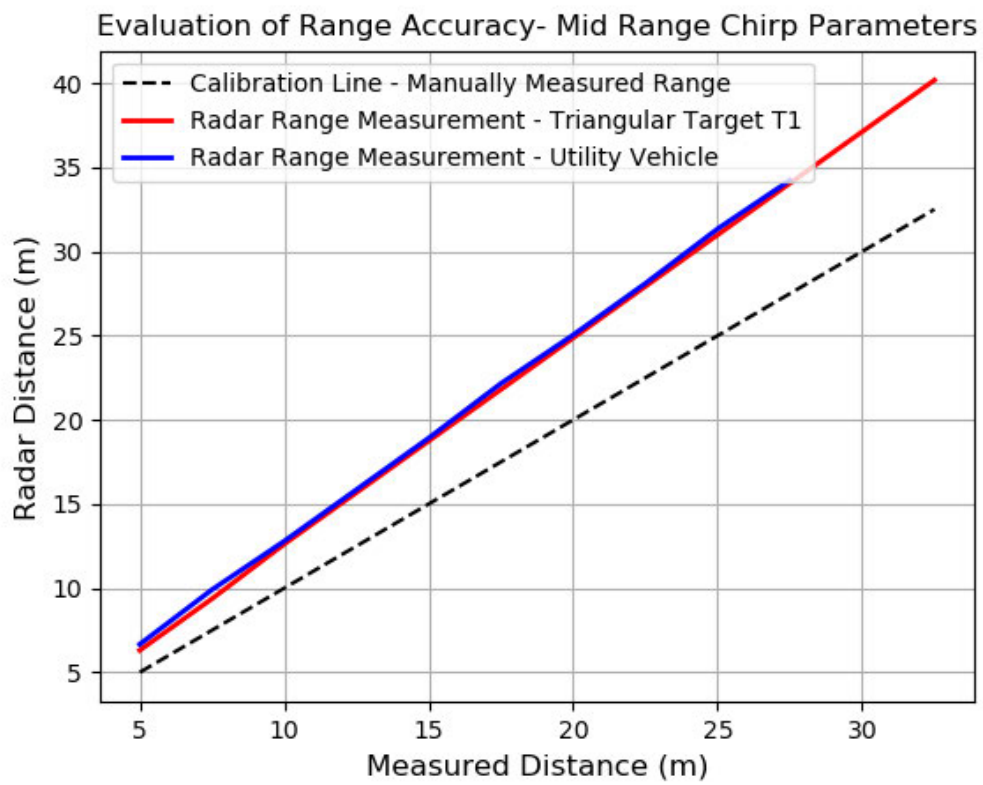


Figure 8.4: Range accuracy using mid-midrange chirp parameters.

8.4 Results - Small Corner Reflectors

Table 8.2: Tabulated triangular corner reflector calculations based on equation 3.1. The listed RCS are smaller than those used in chapter 4.

Triangular Radar Cross Section of small corner reflectors				
Target Designation	Simulated Object	RCS (m^2)	a (mm)	$a\sqrt{2}$ (mm)
T1-Small	Motorcycle	10	78	110
T2-Small	Bicycle	2.5	55	78
T3-Small	Adult	1	43	61
T4-Small	Child	0.2	30	42.5

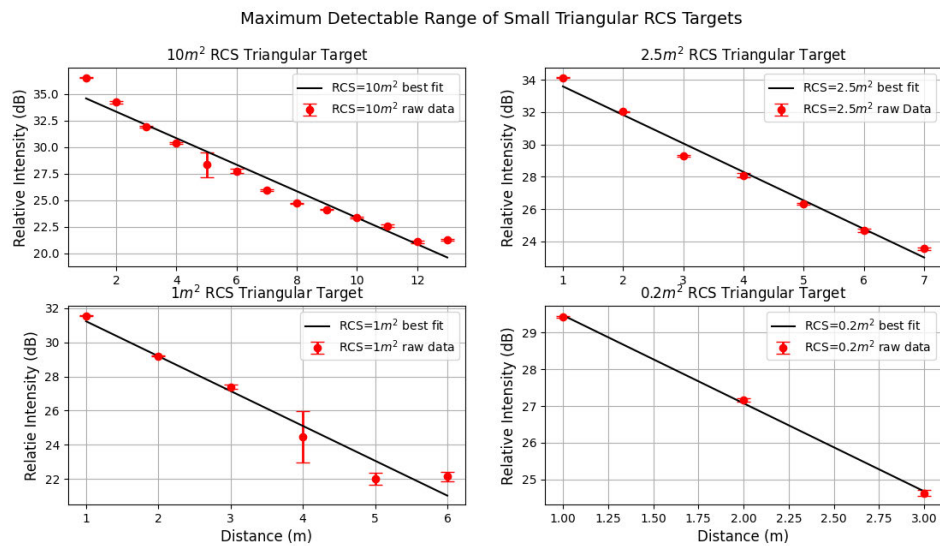


Figure 8.5: evaluation of maximum detectable range and the uncertainty using mid-range chirp parameters and small RCS corner reflectors

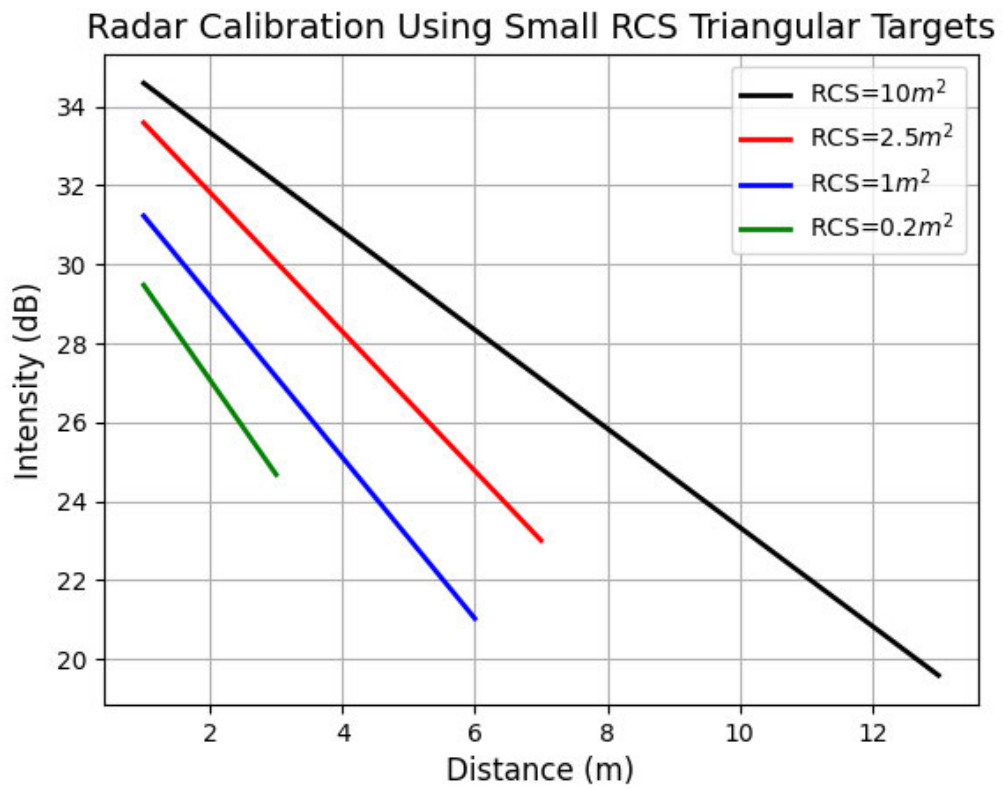


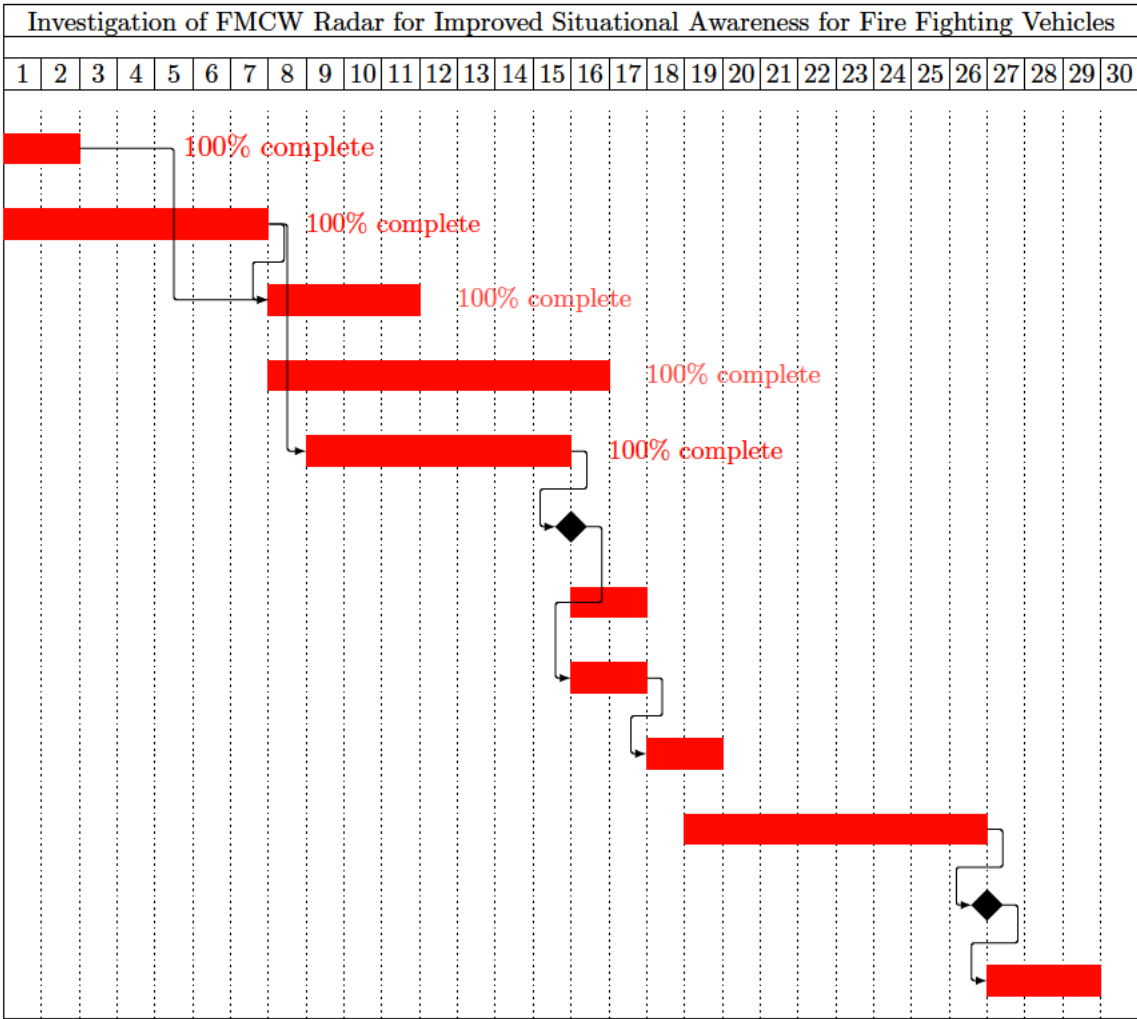
Figure 8.6: Calibration of maximum detectable range using mid-range chirp parameters and small RCS corner reflectors

Chapter 9

Post Processing Example Code

Chapter 10

Project Timeline



Chapter 11

Risk Management Form



For additional information contact Matthew Barrett or Dr Craig Lobsey

Faculty/Division: Faculty of Health, Engineering and Science		School/Unit: Sciences and Engineering (Mechatronics)		
Document number 1.1	Initial Issue date 04/04/2020	Current version 1.1	Current Version Issue date 24/5/2020	Next review date 30/6/2020

Risk management name **Implementation of mm-Wave radar for increased situational awareness and obstacle avoidance on fire trucks.**

Form completed by	Matthew Barrett – Student - Engineering Honours (Mechatronics)	<i>Signature</i> MBarrett	<i>Date</i> 24/05/20
Responsible supervisor/ authorising officer	Dr Craig Lobsey	<i>Signature</i>	<i>Date</i>

Identify the activity and the location of the activity

Description of activity	This risk assessment covers experiments undertaken to identify the feasibility of using affordable, automotive mm-wave radar sensors on fire fighting vehicles to increase situational awareness. The experiments involve mounting an automotive millimetre wave sensor to a vehicle and testing its accuracy in various conditions. The sensor will put out radio wave radiation between 30 -300 GHz. In addition, various pieces of machinery and equipment will be required in order to build the hardware before experiments can begin.
Description of location	Design and build phase – Home office Testing and experimental phase – Parents 300 acre property

Identify who may be at risk from the activity:

This may include fellow workers, visitors, contractors and the public. The types of people may affect the risk controls needed and the location may affect the number of people at risk

Persons at risk	Matt Barrett + People aiding with the experiments
How they were consulted on the risk	Induction / explanation of risk management form. Any person involved will be asked to read this risk management form and sign in the acknowledgment section.

List legislation, standards, codes of practice, manufacturer’s guidance etc used to determine control measures necessary

Work Health and Safety Act 2011
 Work Health and Safety Regulation 2011
 Work safe ACT-Machinery and appliances checklist
 Australian standard AS 3590.2-1990 Screen-based workstations
 Australian Standard AS/NZS 3760: 2010 Test and Tag
 Australian Radiation Protection and Nuclear Safety ACT 2018
 Australian Radiation Protection Standard 3kHz to 300GHz

Possible Hazards (Please tick boxes; include hazards to staff, students, visitors and passers-by)

Materials & Substances		Equipment / Energy Sources		Work Environment		Biomechanics / Manual Handling		Work Organisation	
Chemicals:	<input checked="" type="checkbox"/>	Electrical	<input checked="" type="checkbox"/>	Lighting	<input checked="" type="checkbox"/>	Posture	<input checked="" type="checkbox"/>	Work Space	
Ionising Radiation:		Thermal		Noise/ Vibration	<input checked="" type="checkbox"/>	Load Factors (shape, size)		Assistance available	
Biological		Mechanical	<input checked="" type="checkbox"/>	Dust / Fumes/Vapours	<input checked="" type="checkbox"/>	Repetition		Time Constraints	
Lasers		Kinetic		Access/Egress		Distance		Supervision	
Microwaves		Pneumatic		Confined spaces		Keyboard	<input checked="" type="checkbox"/>	Interactions (public/contractors)	
Waste		Hydraulic		Climate		Duration	<input checked="" type="checkbox"/>	After hours	
Electrical	<input checked="" type="checkbox"/>	Rotational	<input checked="" type="checkbox"/>	Housekeeping	<input checked="" type="checkbox"/>	Lab. instruments		Inadequate rest breaks	
Infrared		Mechanical aids	<input checked="" type="checkbox"/>	Work at height		Individual Factors		Other: (Specify)	
Water		Acoustic		Animals/insects		New Employee			
Ultraviolet (outdoor exposure)		Pressure/Vacuum		Visually demanding		Lone worker	<input checked="" type="checkbox"/>		
Electromagnetic field		Equipment licenses		Flooring (Slips, trips)		Training required			
Non-ionising radiation	<input checked="" type="checkbox"/>	Operator Licenses	<input checked="" type="checkbox"/>	Isolation					

Identify hazards and control the risks.

1. An activity may be divided into tasks. For each task identify the hazards and associated risks. Also list the possible scenarios which could sooner or later cause harm.
2. Determine controls necessary based on legislation, codes of practice, Australian standards, manufacturer's instructions etc.
3. List existing risk controls and any additional controls that need to be implemented

SHADED GREY AREAS

The grey area's must be completed for complex situations where you are unfamiliar with the hazard and risk and how to control it effectively. Many hazards and their associated risks are well known and have well established and accepted control measures. In these situations, it is unnecessary to determine the risk rating, you may simply implement the controls.

Task/ Scenario	Hazard	Associated harm	Existing controls	Any additional controls required?	Risk Rating			Cost of controls (in terms of time, effort, money)	Is this reasonably practicable Y/N
					C	L	R		
Computer related tasks; design, research and writing	Poor Ergonomics Back shoulder and neck pain	Poor workstation setup and poor posture for prolonged periods will result in back neck and shoulder pain	Engineering - Desk set at appropriate height, top of monitors set to be at eyeline, appropriate chair and foot stool Administrative - Break for a walk every 2 hours - Read Australian standard AS3590.2-1990 to understand best practice for screen-based workstation ergonomics.	No	L O W	U n l i k e l y	L O W	NA	Yes
Computer related design and testing of hardware	Electrical Low voltage electronics Sharp objects Electronic components and tools Electrical 240-volt cabling	Low level shock from 12 V battery Abrasions from sharp objects High voltage shock from mains power	Engineering - Isolating power before making adjustments. - Using appropriate fuses or related safety components Administrative - Appropriate training and knowledge - Use appropriately insulated tools - Wear appropriate PPE – Safety glasses Engineering - Use containers and a static proof mat when handling electronic components Administrative - Training on how to appropriately use basic hand tools for electronics Administrative - Check all cabling for damage. If necessary, replace or have tested and tagged. - Only operate equipment on a circuit with a RCD	No	L O W	U n l i k e l y	M E D I U M	NA	Yes

Task/ Scenario	Hazard	Associated harm	Existing controls	Any additional controls required?	Risk Rating			Cost of controls (in terms of time, effort, money)	Is this reasonably practicable Y/N
					C	L	R		
Manufacturing hardware using 3D printing technology and basic fabrication tools	Electrical 240-volt cabling	High voltage shock from mains power	Engineering - Only operate equipment on a circuit with an RCD Administrative - Check all cabling for damage. If necessary, replace or have tested and tagged. - Only operate equipment on a circuit with an RCD	A cardboard or basic enclosure for the 3D printer	M	U	M	NA	Yes
	Temperature Hot 3D printing bed and nozzle	Minor burns and abrasions	Administrative - The 3d printer is isolated and cannot be accessed by anyone other than Matt. - Knowledge of the machine (Don't touch the hot part)						
	Mechanical/Rotational Entanglement	Minor cuts and abrasions	Administrative - The 3D printer is in an isolated location and is also elevated to be easily accessible from a standing position. - Knowledge of the machine (Don't put your hand near the moving parts)						
	Mechanical Sharp metal and hand tools	Minor cuts and abrasions	Administrative - Qualified trade person with training and experience in metal fabrication - Appropriate workspace clear of debris and sharp objects - Wear appropriate PPE including safety glasses, gloves and steel cap footwear.						
Bench top testing of radar system	Non-ionising radiation Indoor radar testing	Not yet known	Elimination - Direct radar out window away from persons or operator. Administrative - Calculations or investigation into the power output of the radar and the allowable specific absorbance rate for the maximum output power	No	M	U	M		
	Poor Ergonomics Back shoulder and neck pain	Poor workstation setup and poor posture for prolonged periods will result in back neck and shoulder pain	Engineering - Desk set at appropriate height, top of monitors set to be at eyeline, appropriate chair and foot stool Administrative - Break for a walk every 2 hours - Read Australian standard AS3590.2-1990 to understand best practice for						
	Electrical 240-volt cabling	High voltage shock from mains power	Engineering - Only operate equipment on a circuit with an RCD Administrative - Check all cabling for damage. If necessary, replace or have tested and tagged.						

Task/ Scenario	Hazard	Associated harm	Existing controls	Any additional controls required?	Risk Rating			Cost of controls (in terms of time, effort, money)	Is this reasonably practicable Y/N
					C	L	R		
Testing of radar while mounted to a tripod	Non-ionising radiation Radar Vehicle testing	Not yet known	Elimination -Radar will always be directed away from people and will only be used to detect a human once all radiation calculations are complete. Administrative - Calculations or investigation into the power output of the radar and the allowable specific absorbance rate for the given power output – See chapter 7 of report for details of calculation	No	M i n o r	U n l i k e l y	L o w	NA	Yes
Performing radar experiments on a RFS vehicle	TBD	TBD	This risk management form will be updated to include any requirements the RFS unit outlines. This may include a completely new risk management documentation process.						

Implementation			
Additional control measures needed:	Resources required	Responsible person	Date of implementation
A new enclosure will be built around the 3D printer as an additional engineering control to minimise the chance of entanglement or burns while the 3D printer is running	Carboard or thin timber	Matt	By 30 April 2020

REVIEW			
Scheduled review date:			
Are all control measures in place?			
Are controls eliminating or minimising the risk?			
Are there any new problems with the risk?			
Review by: (name)			
Review date:			

Acknowledgement of Understanding		
All persons performing these tasks must sign that they have read and understood the risk management document.		
Risk management name and version number:	I have read and understand this risk management form	
Name	Signature	Date

Appendix A. Risk rating procedure

RISK RATING TABLE																																															
Consider the Consequences	Consider the Likelihood	Calculate the Risk																																													
Consider: What type of harm could occur (minor, serious, death)? Is there anything that will influence the severity (e.g. proximity to hazard, person involved in task etc.). How many people are exposed to the hazard? Could one failure lead to other failures? Could a small event escalate?	Consider: How often is the task done? Has an accident happened before (here or at another workplace)? How long are people exposed? How effective are the control measures? Does the environment effect it (e.g. lighting/temperature/pace)? What are people's behaviours (e.g. stress, panic, deadlines) What people are exposed (e.g. disabled, young workers etc.)?	1. Take the consequences rating and select the correct column 2. Take the likelihood rating and select the correct row 3. Select the risk rating where the two ratings cross on the matrix below. VH = Very high, H = High, M = Medium, L = Low																																													
5. Severe: death or permanent disability to one or more persons 4. Major: hospital admission required 3. Moderate: medical treatment required 2. Minor: first aid required 1. Insignificant: injuries not requiring first aid	A. Almost certain: expected to occur in most circumstances B. Likely: will probably occur in most circumstances C. Possible: might occur occasionally D. Unlikely: could happen at some time E. Rare: may happen only in exceptional circumstances	<table border="1"> <thead> <tr> <th colspan="2"></th> <th colspan="5" style="background-color: #4b0082; color: white;">CONSEQUENCES</th> </tr> <tr> <th colspan="2"></th> <th style="background-color: #00008b; color: white;">1</th> <th style="background-color: #00008b; color: white;">2</th> <th style="background-color: #00008b; color: white;">3</th> <th style="background-color: #00008b; color: white;">4</th> <th style="background-color: #00008b; color: white;">5</th> </tr> </thead> <tbody> <tr> <th rowspan="5" style="background-color: #00008b; color: white; writing-mode: vertical-rl; transform: rotate(180deg);">LIKELIHOOD</th> <th style="background-color: #00008b; color: white;">A</th> <td style="background-color: #90ee90;">M</td> <td style="background-color: #ffff00;">H</td> <td style="background-color: #ffff00;">H</td> <td style="background-color: #ff0000;">VH</td> <td style="background-color: #ff0000;">VH</td> </tr> <tr> <th style="background-color: #00008b; color: white;">B</th> <td style="background-color: #90ee90;">M</td> <td style="background-color: #90ee90;">M</td> <td style="background-color: #ffff00;">H</td> <td style="background-color: #ffff00;">H</td> <td style="background-color: #ff0000;">VH</td> </tr> <tr> <th style="background-color: #00008b; color: white;">C</th> <td style="background-color: #add8e6;">L</td> <td style="background-color: #90ee90;">M</td> <td style="background-color: #ffff00;">H</td> <td style="background-color: #ffff00;">H</td> <td style="background-color: #ff0000;">VH</td> </tr> <tr> <th style="background-color: #00008b; color: white;">D</th> <td style="background-color: #add8e6;">L</td> <td style="background-color: #add8e6;">L</td> <td style="background-color: #90ee90;">M</td> <td style="background-color: #90ee90;">M</td> <td style="background-color: #ffff00;">H</td> </tr> <tr> <th style="background-color: #00008b; color: white;">E</th> <td style="background-color: #add8e6;">L</td> <td style="background-color: #add8e6;">L</td> <td style="background-color: #90ee90;">M</td> <td style="background-color: #90ee90;">M</td> <td style="background-color: #90ee90;">M</td> </tr> </tbody> </table>			CONSEQUENCES							1	2	3	4	5	LIKELIHOOD	A	M	H	H	VH	VH	B	M	M	H	H	VH	C	L	M	H	H	VH	D	L	L	M	M	H	E	L	L	M	M	M
		CONSEQUENCES																																													
		1	2	3	4	5																																									
LIKELIHOOD	A	M	H	H	VH	VH																																									
	B	M	M	H	H	VH																																									
	C	L	M	H	H	VH																																									
	D	L	L	M	M	H																																									
	E	L	L	M	M	M																																									

Risk level	Required action
Very high	Act immediately: The proposed task or process activity must not proceed. Steps must be taken to lower the risk level to as low as reasonably practicable using the hierarchy of risk controls
High	Act today: The proposed activity can only proceed, provided that: (i) the risk level has been reduced to as low as reasonably practicable using the hierarchy of risk controls and (ii) the risk controls must include those identified in legislation, Australian Standards, Codes of Practice etc. and (iii) the document has been reviewed and approved by the Supervisor and (iv) a Safe Working Procedure or Safe Work Method has been prepared and (v) the supervisor must review and document the effectiveness of the implemented risk controls
Medium	Act this week: The proposed task or process can proceed, provided that: (i) the risk level has been reduced to as low as reasonably practicable using the hierarchy of controls and (ii) the document has been reviewed and approved by the Supervisor and (iii) a Safe Working Procedure or Safe Work Method has been prepared.
Low	Act this month: Managed by local documented routine procedures which must include application of the hierarchy of controls.